Analysis and Design of Rocking Mechanisms

by

Tamás Ther

Master of Science, Architectural Engineer (2010)

Budapest University of Technology and Economics

Faculty of Architecture

May 2017

Contents

Table of Figures

Acknowledgements

Firstly, I would like to thank my supervisor, Prof. László P. Kollár for his persistent, patient and calm guidance and assistance. We always discovered the ways out of dead-ends and found the common ground to continue our work.

My wife, Zsuzsi, who encouraged and put up with me, when I was on the verge of dropping the whole project. My parents and my brothers for their support and constant interest.

Special thanks to my colleagues at the department, András Sipos, István Sajtos, Péter Várkonyi and Tamás Baranyai for their assistance. I could always count on them, even if it came to answering the most basic questions.

The members of our research group, Zsuzsa Borbála Pap, Attila Joó and Ádám Zsarnóczay for their support and constructive criticism. I am particularly grateful to Ádám for his patient instructions, while I was learning OpenSees and working with Superman, as well as for his feedback on my papers.

Ottó Sebestyén, who helped me to bring the old shaking table back to life for the laboratory tests, and Péter Károly Juhász for his support.

I would like to particularly thank Árpád Barsi for his guidance during developing the image-processing algorithm for the experiments.

Last but not least, Miklós Armuth and Dezső Hegyi for the design and expert opinion assignments, which helped me to provide for my family during this lengthy PhD process.

Abstract

This dissertation presents a simple design method to predict the safety of rocking multi-block columns. As the background of the design method Housner's refined impact model and a new model for multi-block columns subjected to earthquakes, which contains an impact and an opening model are presented.

The reasons of the well-known fact that rocking block experiments show lower energy loss during impact than it is predicted by Housner's impact model is investigated. It is found that a reasonable explanation for the difference is that in the original model the best case scenario was assumed: that impact occurs at the edges, which results in the maximum energy loss. In reality, due to the unevenness of the surfaces, or due to the presence of aggregates between the interfaces, rocking may occur with consecutive impacts, which reduces the energy loss. This hypothesis is also verified by experiments.

The new 2D column model is purely mechanical: assuming rigid blocks and classical (inelastic) impact. Both in the impact and in the opening model all the possible opening configurations are investigated, since it is shown that in many practical cases unexpected patterns may occur. The effect of energy dissipation during impact is investigated. Using the model in accordance with the literature it is found that monolithic blocks are more vulnerable to overturning than multi-block systems.

With the aid of the column model it is shown that an earthquake can be reasonably well represented for overturning by two parameters: the peak ground acceleration and the replacement impulse duration. The Overturning Acceleration Spectra of rigid blocks is presented for 100 different earthquake records. Based on the response of the elements a new parameter, the "replacement impulse duration" is defined, that leads to a simple design method to predict the safety of rocking blocks.

Chapter 1 Introduction

Historic masonry and stone buildings are vulnerable to earthquakes. Most of the churches built in Hungary in the XII-XIXth centuries contain stone or brick columns, walls and arches. Many of them were severely damaged by moderate ground motions. For example, in 1956 the vaults of a baroque church in Taksony was collapsed during the Dunaharaszti earthquake, M5.6 (Szeidovitz 1984). In the archive photos (Fig. 1) it is clearly visible, that the motion of the arches were so big that the vaults collapsed, while the arches themselves became seriously damaged but were not destroyed. This is the reason that in the investigation of stone or brick buildings both the stability of the structure and the motions during the excitation must be examined. It is also important to note that these structures were not designed for earthquakes, however today they must be investigated for the expected seismic event.

Fig. 1 The ruined *Szent Anna* parish church after the earthquake in Dunaharaszti, 12th Jan. 1956 (Historia Domus 1956)

Static analysis of brick or stone structures are well explored and they are usually based on the thrust line analysis (see e.g. the fundamental paper of Heyman (1966)) with the aid of which a pushover analysis can also be performed. For earthquake design these methods are inapplicable. To illustrate this, we recall Housner's (1963) statement that these structures subjected to earthquakes show a clear size effect (the smaller the structure, the more vulnerable for earthquakes) which can not be modelled with the static analysis.

It is well known, that the classical analysis used for the design of regular buildings, such as the Response Modal Analysis (RMA) or even the time history analysis of elasto-plastic structures are not directly applicable for masonries, where the “rocking” of the blocks (opening and closing with impact) plays an important role in the nonlinear response of masonry structures (Makris and Konstantinidis 2003). The main reason that RMA is not applicable is that these structures do not have a definite period of vibration, since motion occurs by the opening and closing of the cracked interfaces (the elastic deformations are negligible) and the length of “period” depends on the opening of the interface.

As a rule, we may say that there is no generally accepted method to analyze and design these kinds of structures.

In this thesis we will make three important steps to reach a design methodology:

- modelling of single (rocking) blocks for earthquakes,
- modelling of columns consisting of rigid blocks, subjected to earthquakes,
- develop a design method to evaluate rocking structures.

The literature summary presented below follows these major steps.

Modelling of single blocks

Housner (1963) published his classical paper more than five decades ago, in which he presented a simple model for the rocking rigid block (Fig. 2). He investigated a block which rotates around corner *A*, then – when the block reaches the vertical position – impact occurs, and the block rotates further around corner *B*. Assuming identical angular momentum about corner *B* before and after the impact (Fig. 2), he determined the angular velocity after impact, ω_a (Fig. 2c) as a function of the geometry and the angular velocity before impact, ω_b (Fig. 2a):

$$\omega_a = \mu_{\text{Hous}}\omega_b, \qquad \mu_{\text{Hous}} = \frac{2h^2 - b^2}{2h^2 + 2b^2} \tag{1}$$

where ω_b and ω_a are the angular velocities before and after rocking, h and b are the dimensions of the block (Fig. 2a), μ is the angular velocity ratio.

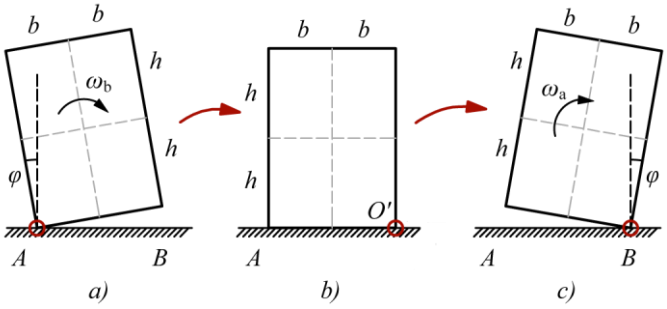

Fig. 2 Housner's model for a rocking block

The square of the angular velocity is proportional to the kinetic energy of the rocking block, and hence at every impact there is an energy loss. The relative loss in kinetic energy during rocking can be calculated as:

$$\eta = \frac{\omega_b^2 - \omega_a^2}{\omega_b^2} = 1 - {\mu_{Hous}}^2 \tag{2}$$

The motion of a rocking block – subjected to gravity load only – according to Housner's model is shown in Fig. 3. Note that both the amplitude and the time between impacts decrease with time.

The rocking block was investigated experimentally by several researchers: Anooshehpoor and Brune (2002) used timber blocks, Prieto-Castrillo (2007) and Ther and Kollár (2017d) granite, Aslam et al. (1980) and Ma (2010) concrete, Lipscombe and Pellegrino (1993) used steel elements. In almost every case, it was found that in the experiments the energy loss (and the decrease in angular velocity) is smaller than the one predicted by Housner's model (Fig. 3). The results are shown in Table 1 and in Fig. 4.

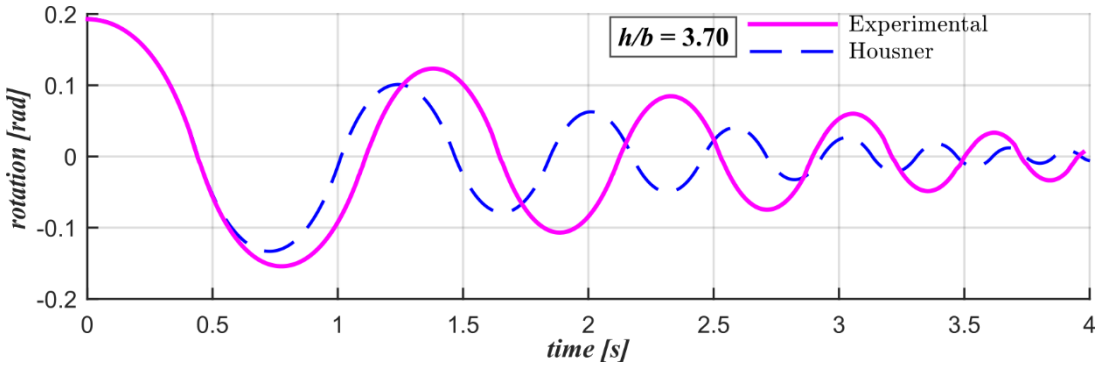

Fig. 3 Typical time- displacement curve of a rocking block according to Housner's model (dashed line), and according to our experiment (solid line).

In case of the experiments of Elgawady et al. (2011) rocking did not occur freely but through a steel mechanism, which was applied on the system. This is the reason that this experiment was not included in Fig. 4. Aslam et al. (1980) reported high slips (and, accordingly, high energy loss) during the experiments, which explains that in this case the energy loss is higher than in case of Housner's model.

Researchers gave different explanations for the significant differences between the results of the experiments and the model (see the summary of Lagomarsino (2015)), and several improvements were suggested. Augusti and Sinopoli (1992) and Kounadis (2015) took into account the sliding between the block and the base, which, especially for small aspect ratios, is a necessary and important improvement. Note, however, that it cannot explain that the model underpredicts the energy loss (Table 1). A possible explanation assumes that the impact is neither plastic nor elastic: Lipscombe and Pellegrino (1993) stated that the bouncing is significant for short blocks. They insert the coefficient of restitution into Housner's equations to reach an agreement with the experiments, where the bouncing of the element was detected. This effect has been experimentally tested by Elgawady et al. (2011), by investigating the material of the surface of the base under the rocking element. Ma (2010) ran over 400 experimental tests with a built-in steel mechanism that prevents sliding to explain the discrepancy. In conclusion, he stated that the experiments have demonstrated that despite the very simple appearance of free rocking motion, highly complex interactions play an important role. To overcome the differences between the model and the experiments, some of the researchers suggested to use an angular velocity ratio (μ) which agrees with the experiment and not with Housner's model (Priestley et al. 1978; Aslam et al. 1980; Lipscombe and Pellegrino 1993; Anooshehpoor and Brune 2002; Elgawady et al. 2011).

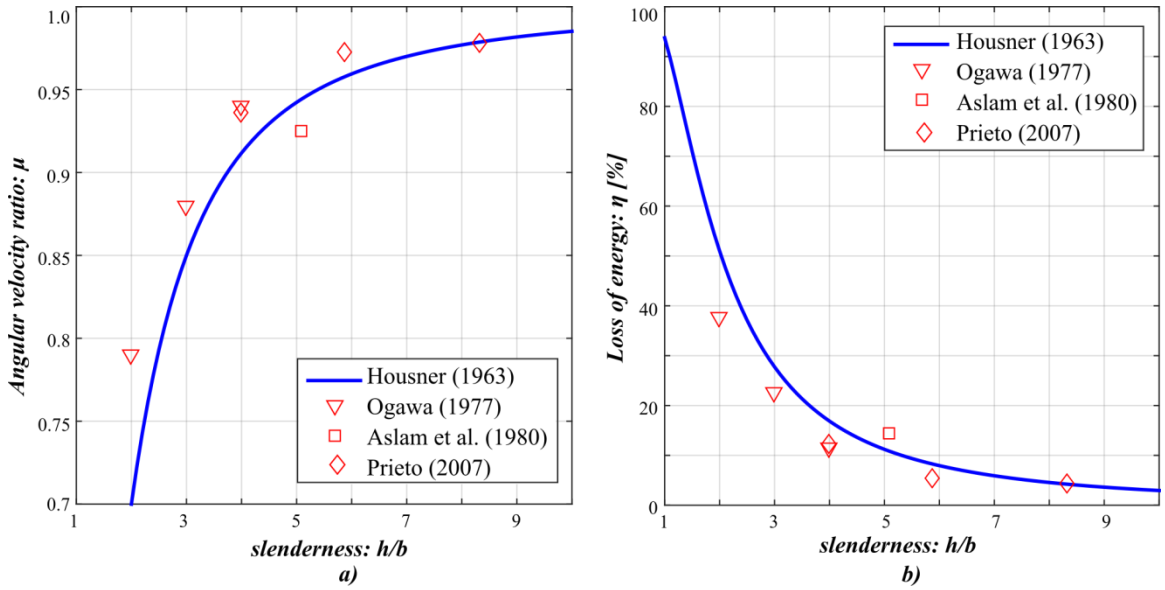

Fig. 4 The reduction in speed (μ) and the loss of kinetic energy ($\eta_{Hous}=1-\mu^2_{Hous}$) for different aspect ratios. Experimental results (Ogawa 1977; Aslam et al. 1980; Prieto-Castrillo 2007) compared with Housner's model. (Aslam reported significant slips, which explains the high energy loss.)

Note that in spite of the presented inaccuracies Housner's model is widely applied because of its simplicity and physical clarity. Numerical solutions were developed to follow the motion (Augusti and Sinopoli 1992; Lipscombe and Pellegrino 1993; Prieto et al. 2004; Kounadis 2015), and with the aid of these, several authors determined overturning curves (see Chapter 5) to analyse the stability of a single rocking block (Housner 1963; Yim et al. 1980; Ishiyama 1982; Hogan 1989; Sinopoli 1991; Shi and Anooshehpoor 1996; Psycharis et al. 2000; Makris and Konstantinidis 2003; Peña et al. 2006; Peña et al. 2007; Prieto-Castrillo 2007; Makris and Vassiliou 2012; Voyagaki et al. 2013a; Voyagaki et al. 2013b; Vassiliou et al. 2016). Oppenheim (1992) extended this for the investigation of arches and De Lorenzis (2007) defined stability maps for impulse-ground motions. Housner's model was also extended to investigate non-symmetric monolith blocks (Shi and Anooshehpoor 1996; Di Egidio and Contento 2009; Zulli et al. 2012) and two (Psycharis 1990; Spanos et al. 2001) or multi degree of freedom structures (Ther and Kollár 2014; Ther and Kollár 2017b).

Housner's model is a very important element of the analysis of structures subjected to earthquakes, where cracks may open and close during excitations. These are, for example: columns, walls and arches made of masonry, stone or unreinforced concrete blocks (Fig. 5).

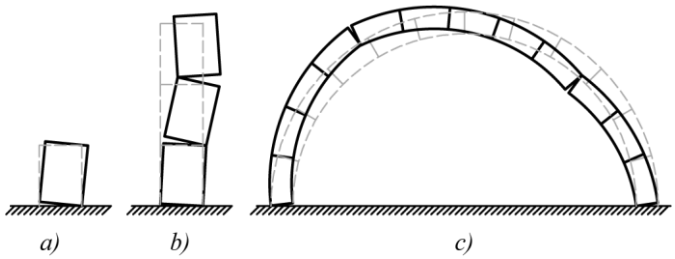

Fig. 5 Columns and arches, where Housner's model is applied

Modelling of columns consisting of rigid blocks

Masonry and stone columns are important structural elements. Their modelling must include the possible openings and closings of the cracks between the blocks, which require the use of an impact model.

Single-block columns were first investigated by Housner (1963), who derived a formula for the change in velocity of rocking elements.

The motion of multi-block columns, when the locations of the open interfaces are given, were investigated by Prieto-Castrillo (2007), who described a robust method for predicting their motion between two consecutive impacts.

For the impact of multi-block columns only a few mechanical models are available. Housner solved the single block, Psycharis (1990) presented a model for the two-block mechanism. His solution is accurate when at impact all the elements are vertical, and approximate for inclined elements. This solution was generalized by Spanos et al. (2001) for the impact of a two-block inclined system. As far as we know no mechanical model of impact is available for columns with more than two blocks. (It might be worthwhile to mention that Housner's model was generalized for arches (Oppenheim 1992; De Lorenzis 2007; DeJong et al. 2008; DeJong 2009). The presented four-hinge mechanism is a one degree of freedom system.) The opening pattern during impact was investigated by Psycharis (1990) for a two-block system.

An alternative method to investigate the multi-block system is the discrete element method (DEM) (Winkler et al. 1995; Psycharis et al. 2000; Komodromos et al. 2008; DeJong 2009; Tóth et al. 2009; Dimitri et al. 2011; Lengyel and Bagi 2015) or other commercially available softwares, where the properties of the contact interfaces between the rigid blocks must be defined (Konstantinidis and Makris 2005). By setting certain parameters they seem to be robust methods for investigation multi-block columns. Using the discrete element method it was observed that monolithic blocks are more vulnerable to overturning than multi-block systems with the same overall dimensions (Psycharis et al. 2000; Dimitri et al. 2011).

Design methodology of rocking mechanisms

Overturning of rigid blocks on rigid foundations subjected to earthquakes has been investigated by several researchers. For the design of overturning of blocks the following approaches were suggested:

(1) to evaluate a limit (or push over) analysis;

(2) to apply an equivalent viscous damping model to take into account the impact during rocking;

(3) to determine a single replacement pulse (Fig. 6) from the earthquake record, and then, evaluate the element with the overturning curve (OC) for the pulse; or

(4) to determine the response of the block for a given earthquake by time history analysis.

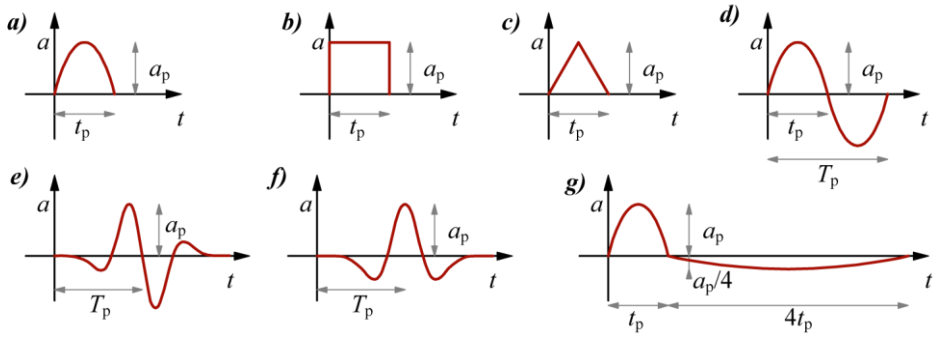

Fig. 6 Suggested signal shapes for generating OC (see (Makris and Vassiliou 2012) for signals e and f)

The limit analysis of rigid blocks, or structures made of rigid blocks (Livesley 1978) subjected to horizontal loads is relatively simple. However, it may be very conservative and it does not show the size effect for rocking blocks subjected to earthquakes, which was observed and also analytically proven by Housner (1963) in his classic paper: larger structures are less vulnerable to overturning than smaller ones.

Priestley et al. (1978) suggested to use equivalent viscous damping to take into account the impact in the analysis. Makris and Konstantinidis (2003) criticized this approach and stated that rocking structures cannot be replaced by 'equivalent' single degree of freedom (SDOF) oscillators.

Several researchers recommended replacing earthquake records by simple signals (Fig. 6a-c). Housner (1963) and Yim et al. (1980) investigated a half sine and a single rectangular pulse, Voyagaki et al. (2013b) investigated the effect of a range of idealized single-lobe pulses, while Ishiyama (1982); Augusti and Sinopoli (1992); Anooshehpoor et al. (1999); Zhang and Makris (2001); Makris and Vassiliou (2012); Dimitrakopoulos and DeJong (2012) and Dimitrakopoulos and Fung (2016) applied full-cycle pulses where impact plays an important role (Fig. 6d-f).

Voyagaki et al. (2013a) suggested using a single-lobe triangular pulse with a duration defined by Baker (2007), and it was shown numerically that this pulse gives a conservative solution for the investigated earthquakes. There are several recommendations on the calculation of the shape and duration of simple signals (Mavroeidis and Papageorgiou 2003; Baker 2007; Vassiliou and Makris 2011; Mimoglou et al. 2014), see also the literature review of Lagomarsino (2015).

To evaluate the safety of the elements the overturning curve (acceleration as a function of duration) was introduced first by Housner (1963) for a half sine and a single rectangular pulse, then for other shapes by other researchers (Yim et al. 1980; Ishiyama 1982; Augusti and Sinopoli 1992; Anooshehpoor et al. 1999; Zhang and Makris 2001; Makris and Vassiliou 2012; Dimitrakopoulos and DeJong 2012; Voyagaki et al. 2013a; Voyagaki et al. 2013b; Dimitrakopoulos and Fung 2016) and harmonic shaking by Spanos and Koh (1985) and Hogan (1992). It was also shown that for complex signals the overturning curve may contain bays and islands (Zhang and Makris 2001; Makris and Vassiliou 2012; Dimitrakopoulos and DeJong 2012; Voyagaki et al. 2013a; Dimitrakopoulos and Fung 2016; Ther and Kollár 2017a). (This overturning curve is called overturning acceleration spectrum by some researchers (Zhang and Makris 2001; Makris and Vassiliou 2012). In this thesis the latter name is used for a modified diagram, see subsection 5.1.1.)

Researchers investigated overturning for white noise-based artificial earthquake records (Housner 1963; Priestley et al. 1978; Aslam et al. 1980; Yim et al. 1980; Ishiyama 1982; DeJong 2012) and also for real earthquakes (Ishiyama 1982; Makris and Konstantinidis 2003; Peña et al. 2006; Peña et al. 2007; DeJong 2012; Makris and Vassiliou 2012; Voyagaki et al. 2013a). Makris and Vassiliou (2012) showed that the effect of a near-fault, pulse-like earthquake can be replaced by a single rectangular pulse with properly chosen pulse duration. Ther and Kollár (2017a) have shown that fullness of the replacement pulse and the secondary pulse have a major effect on the OC.

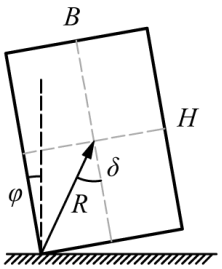

Fig. 7 Geometry of the rigid block (the aspect ratio is: $H/B=\cot\delta$, moment of inertia about the corner point is $\Theta = \frac{4}{3}R^2m$, where m is the total mass)

As mentioned above, the overturning curve of a single rectangular block subjected to a half sine pulse was introduced by Housner (1963). For a given block and a given signal shape (e.g. a simple half sine) it can be defined as the curve which separates the safe and unsafe regions on the a_p, t_p plane where a_p is the maximum intensity of the main pulse lobe (acceleration) and t_p is the duration of the pulse (Fig. 8a). If the a_p and t_p parameters of a pulse correspond to a point on the left side of the curve, it will not overturn the block. If $a_p<a_{p,min}$ the block will not move at all, where (Fig. 7)

$$a_{\mathrm{p,min}} = g \tan \delta \tag{3}$$

and g is the acceleration of gravity. The OC can be calculated for other signal shapes (Zhang and Makris 2001; Makris and Konstantinidis 2003; Makris and Vassiliou 2012; Dimitrakopoulos and DeJong 2012; Voyagaki et al. 2013a; Voyagaki et al. 2013b; Dimitrakopoulos and Fung 2016), examples for two and three consecutive half sines are shown in Fig. 8b and c (t_p is the duration of the half sine). Within the unsafe region there are (narrow) safe bays. In this case (or for more complex signals, where there are several bays and islands) a single envelope can be used for design purposes. All three figures show that for a given block both a shorter pulse with higher intensity and a longer pulse with lower intensity can cause the overturning of the block. The rotations of the block for different pulses are presented in Fig. 9.

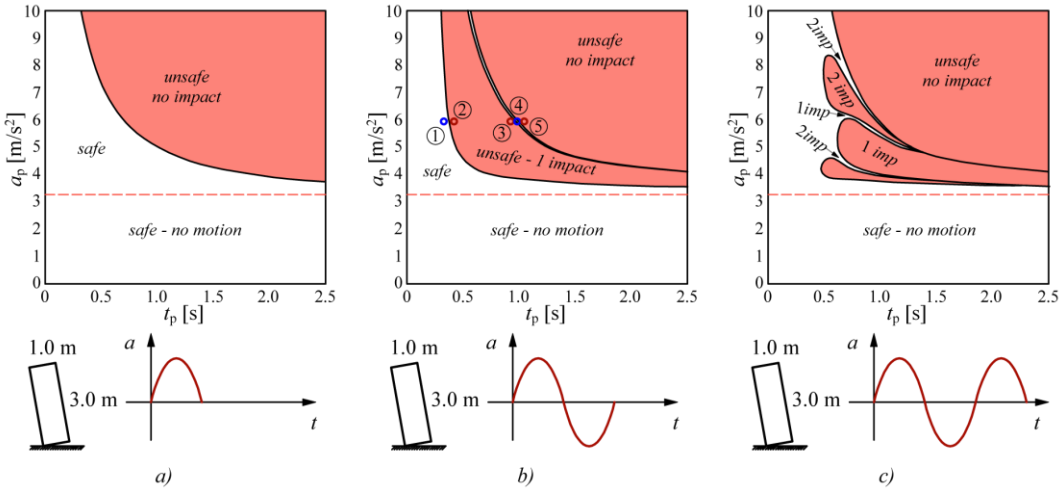

Fig. 8 Overturning curve (OC) for a single block subjected to a half sine pulse (a) a full sine signal (b) and for a signal of three half sines (c)

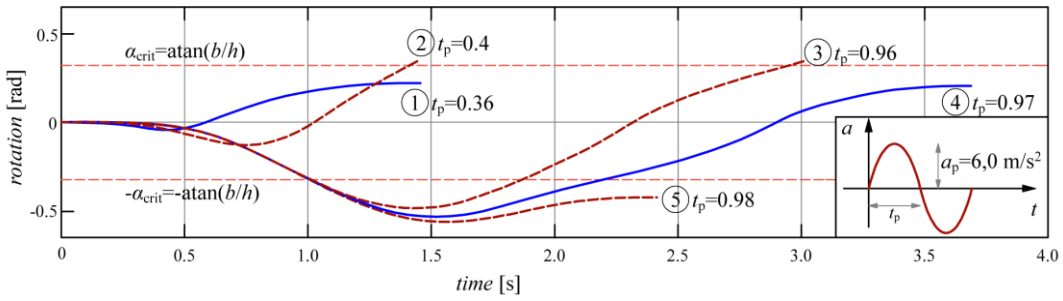

Fig. 9 Motion of the rocking block for different impulses. (See the numbered dots in Fig. 8b.)

Chapter 2 Problem statement

Modelling of single blocks

As we stated in Chapter 1 (see Fig. 3 and Fig. 4) experiments show lower energy loss during impact than it is predicted by Housner's model, which means that – as a rule – Housner's model is not conservative. Although, in practice, fudge-factors may be successfully used to obtain proper results, it is worthwhile to find a physical explanation for the difference, and – if possible – to have an improved mechanical model.

Table 1 Experimental results (Ogawa 1977; Prieto-Castrillo 2007; Elgawady et al. 2011) compared with Housner's model. η_{Hous} is the relative energy loss. (η_{Hous} was calculated by Eq.(1) and (2) except the last one, where Eq.(A3) and (2) were used).

Author	Material of the block	$2h$	$2b$	$2b_2$	h/b	Loss in Energy	
						$\bar{\eta}$	η_{Hous}
Ogawa (1977)	timber	200	100		2.00	37.6%	51.0%
Ogawa (1977)	timber	300	100		3.00	22.6%	27.8%
Ogawa (1977)	timber	400	100		4.00	11.6%	16.9%
Aslam et al. (1980)	concrete block with aluminum plate	771.5	152		5.08	14.4%	10.9%
ElGawady et al. (2011)	concrete block with steel plate	950	190		5.00	15.6%	11.2%
Prieto (2007)	granite	1000	250		4.00	12.4%	16.9%
Prieto (2007)	granite	1000	170		5.88	5.3%	8.2%
Prieto (2007)	granite	1000	120		8.33	4.4%	4.2%
Prieto (2007)	granite	500	246	160	2.03	14.0%	25.2%

Our aim is to give a physical explanation why Housner's model overpredicts the loss in energy, and to develop a physical model which agrees better with the experiments.

Modelling of columns consisting of rigid blocks

As can be seen in the Introduction mechanical models are available for single blocks (Housner 1963) and two-block columns (Psycharis 1990; Spanos et al. 2001), no model is available for multi-block columns with more than two blocks.

Available FE codes (e.g. ANSYS, OpenSees, etc.) might be able to calculate the motion of blocks including the deformability of the elements and the geometrical nonlinearities. However, no proper "impact" and "opening" routines are available, hence these codes must be combined with "opening" and "impact" models. We did so and connected OpenSees with our own MatLab "opening" and "impact" routines (described in section 3.2), however, we had numerical difficulties. The reason was the high frequency axial vibration of the elements (also mentioned by Vassiliou et al. (2016)), which made it difficult to verify the eccentricities of the normal forces and, in a few cases, resulted in unstable solutions.

This is why we decided to develop our own code with a low number of degrees of freedom, to obtain a robust, reliable tool to calculate the response of multi-block columns assuming rigid body theory.

We consider a column which consists of rigid (brick or stone) blocks. It is subjected to an arbitrary excitation. During motion, any interface may split open or close and the crack pattern may change with time (Fig. 10). We wish to develop a model, which is capable of following the response of the structure.

In the analysis only the planar displacements of the columns are taken into account.

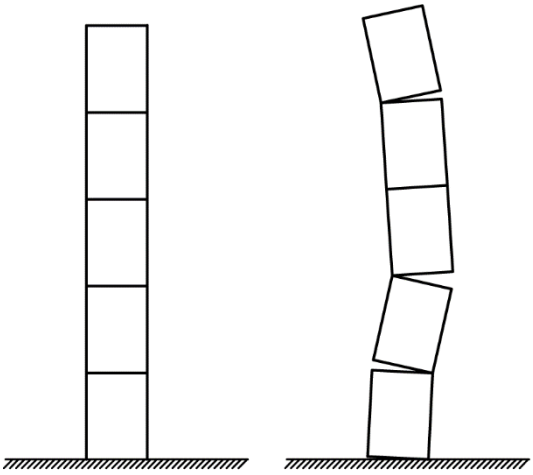

Fig. 10 Multi-block column

Damping during motion is neglected, however, at the closing of interfaces there is a loss in energy due to inelastic impact (Housner 1963).

Using the new model we wish to investigate the observation made by Psycharis et al. (2000) and Dimitri et al. (2011) that monolithic blocks are more vulnerable to overturning than multi-block systems.

Design methodology of rocking mechanism

For the design of blocks for single pulse-like signals the overturning curve (OC) was introduced by Housner (1963).

We consider a multi-block column (Fig. 10), which is subjected to base (earthquake) excitation. We wish to develop a design methodology to determine whether the structure is safe. Similarly to the response spectrum analysis (RSA), where the design can be performed on the basis of the response spectrum, we wish to determine the required design parameters (or curves) which can be applied for the checking of overturning of columns. We wish to give recommendations on how the earthquakes (both near field and far field types) can be represented by a few parameters, in such a way that the responses of rigid columns calculated by time history analysis and by the developed procedures are close to each other or at least the latter one can be used as a conservative approximation to predict overturning.

Chapter 3 Method and modelling

In the following subsections the modelling of single and multi-block structures are presented.

3.1 Refinement of Housner's rocking model

First, we apply a simple modification on Housner's classical model. It is assumed that the surface of the block (or the ground surface) is not perfectly smooth, but there is a small bump (or aggregate) in the middle (Fig. 11a). In this case the rocking occurs with two impacts (Ther and Kollár 2014). Before rocking the block rotates around corner *A*. Then, impact occurs, and the

- block rotates around point *C* (bump or aggregate). Following that a
- second impact occurs and the block rotates around corner *B*.

If the size of the bump (or aggregate) is small, then the time between the two impacts is also small, however, the final angular velocity is higher than in Housner's model. (This can be shown simply by applying Housner's model twice. See Eq.(A8) in Appendix A.)

If there are two bumps (Fig. 11b), rocking occurs with three impacts, and if there are *n* bumps (which form a convex surface), rocking occurs in *n*+1 impacts. Fig. 12 shows the loss in kinetic energy as a function of the aspect ratios with 1, 2, ...100 bumps. If the number of bumps goes to infinity, the block will "roll" and the energy loss is zero.

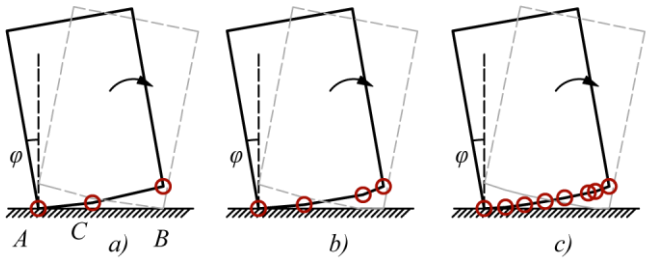

Fig. 11 Rocking block. a: one bump in the middle, b: two bumps, c: several bumps

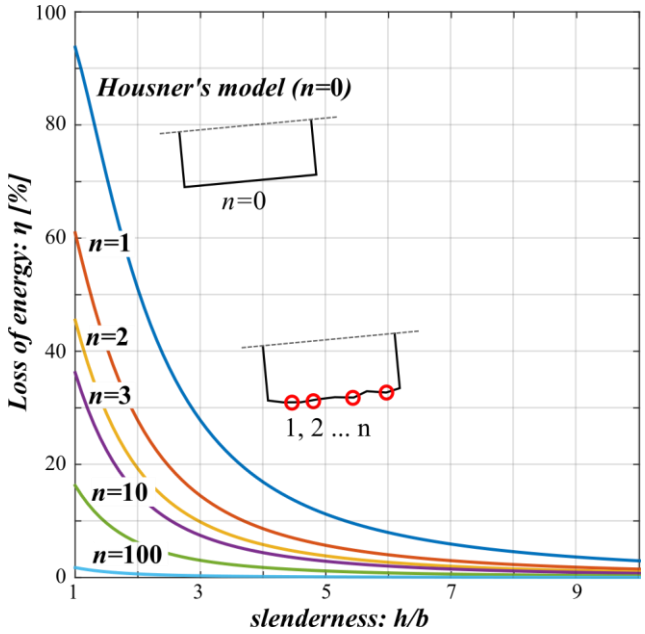

Fig. 12 Loss in kinetic energy as a function of slenderness of the block for *n* bumps

In reality, there is no perfect surface (Fig. 13a), and as it was shown above, even a small unevenness of the surface (bump or aggregate) changes the loss in the kinetic energy during rocking significantly.

We assume that the main reason that Housner's model overpredicts the loss in kinetic energy is the following:

- impact does not occur purely at the edges of the blocks (Fig. 13b), rather – in consecutive steps – at bumps and then at the edges (Fig. 13c).

We suggest that Housner's model can be improved by taking into account these additional impacts during rocking.

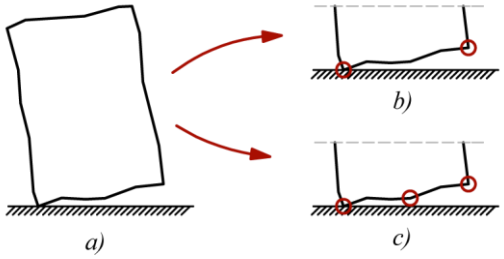

Fig. 13 Comparison of Housner's model and the modification with an additional bump in the middle

To evaluate the above hypothesis experiments were carried out, which are presented in subsection 4.1. In addition, we investigated some of the experiments available in the literature.

To demonstrate the importance of the improvement of Housner's model we simulated the motion of a block subjected to a base excitation recorded at the Northridge earthquake (Fig. 14a, 1994, NORTHR/MUL009 component). The aspect ratio of the element is 4, while its diagonal is 2.6 m, hence its sizes are b=0.315 m and h=1.261 m. When Housner's classical model is applied (Fig. 14b) the block does not overturn, its maximum inclination is about 80 percent of the neutral position (at about 9 s). When the above improved model is applied (with one additional bump), which agrees better with the experiments (see section 4.1), it can be observed that the inclination of the block becomes bigger and bigger during the excitation, resulting in overturning at about 11 s.

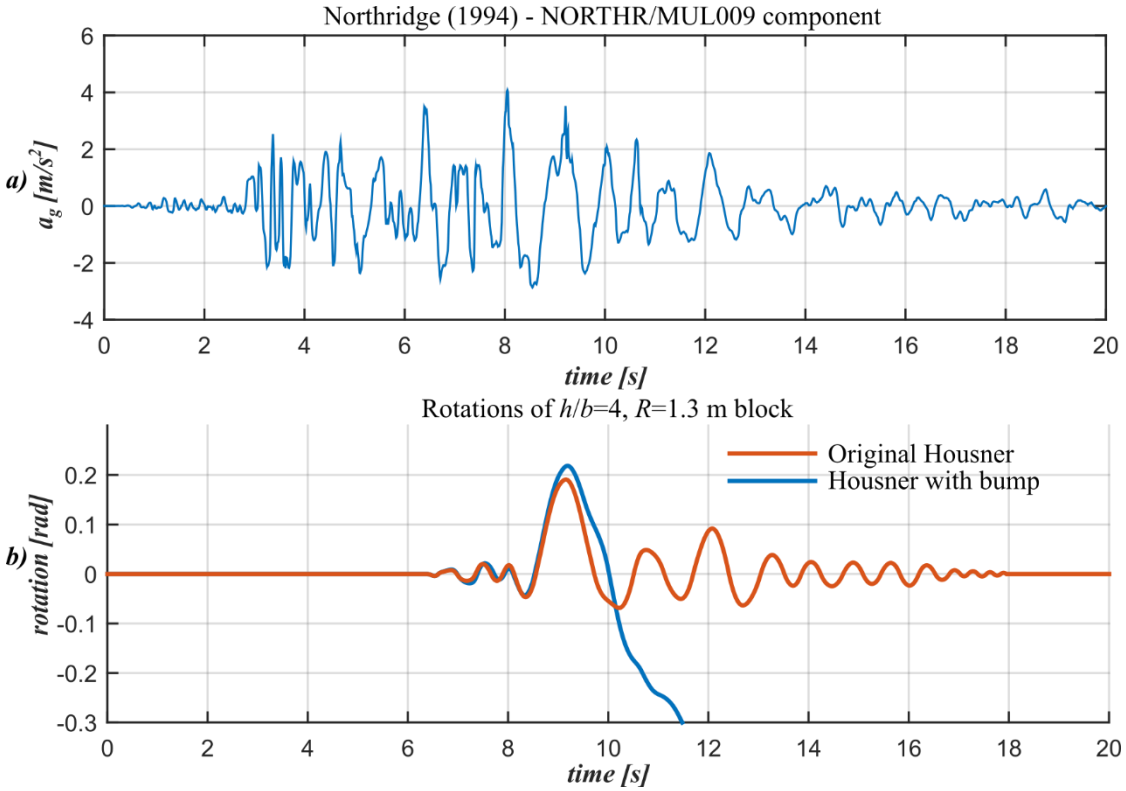

Fig. 14 The rocking motion of a block considering the original Housner's model and the proposed improvement

3.2 Opening and impact model for multi-block structures

It is assumed that the column contains rigid elements and the motion occurs by the rotations at the cracked interfaces between two blocks (Fig. 10). In the following models are presented for the opening and closing (impact) of interfaces. In theory the program may take into account the sliding of the elements, however, a sufficiently high friction coefficient was assumed, and (except for the case of tension) failure was always governed by overturning, not by sliding.

3.2.1 The mechanical model

We consider a multi-block cantilever structure where all the blocks are rigid. The adjacent blocks may move together (Fig. 15a) split open clockwise (Fig. 15b) or counterclockwise (Fig. 15c).

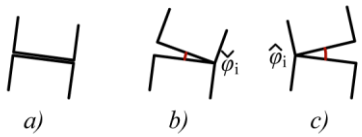

Fig. 15 Opening possibilities of an interface (closed (a), open clockwise (b) and counterclockwise (c))

Since only one of the three possibilities may occur for every possible opening-configuration a new formulation should be given. The key element of our model is that at the interfaces both clockwise and counterclockwise rotations are considered.

When there are n_b blocks and n_b interfaces freely moving in 2D, the number of independent motions is $2n_b$ (Fig. 17b),

$$\boldsymbol{\varphi} = \{\check{\varphi}_1 \ \dots \ \check{\varphi}_{n_b}, \hat{\varphi}_1 \dots \ \hat{\varphi}_{n_b}\}^T, \tag{4}$$

where due to geometrical constraints

$$\check{\varphi}_i \leq 0, \quad \hat{\varphi}_i \geq 0 \ \rightarrow \text{no overlapping.} \tag{5}$$

This formulation has two advantages:

1) The dynamic problem must be formulated only once and the actual configuration is obtained by setting some of the displacements (at least n_b) to zero. More importantly:
2) during impact the interface where closing occurs may open up in the other direction (Fig. 16a), and hence in the impact model (see section 3.2.3) both clockwise and counterclockwise rotations must be included.

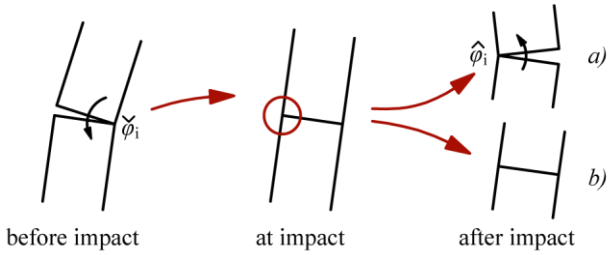

Fig. 16 Possible motions of an interface after impact

For the formulation between impacts only one of the three cases (Fig. 15) may occur in the same time and only one of each $\check{\varphi}_i - \hat{\varphi}_i$ pair can be nonzero (Eq.(5)).

The equation of motion for the entire problem can be written as

$$\mathbf{M}_c \ddot{\boldsymbol{\varphi}} = \mathbf{m}, \tag{6}$$

where $\ddot{\boldsymbol{\varphi}}$ is the second derivative of the rotation vector (Eq.(4)) with respect to time, $\mathbf{m}$ is the load vector and $\mathbf{M}_c$ is the mass matrix. To formulate the problem, it is easier to start with horizontal and vertical displacements and vertical (gravitational) and horizontal (earthquake) loads. The transformation of the equation of motion, when the displacements are replaced (the horizontal and vertical displacements by φ rotations) are described in Appendix C, where $\mathbf{M}_c = \tilde{\mathbf{M}}$, $\ddot{\boldsymbol{\varphi}} = \ddot{\tilde{\mathbf{u}}}$ and $\mathbf{m} = \tilde{\mathbf{p}}$. The load vector $\mathbf{m}$ contains $2n_b$ moment couples which are determined from the base excitation. A numerical example is presented in Appendix C.

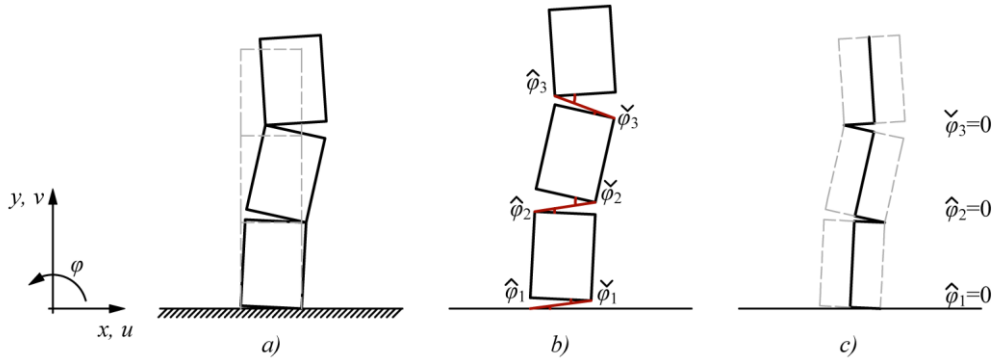

Fig. 17 The degree of freedom of the model. One possible case of a three-block system (a), the theoretically possible motions (b) and the choice of the zero and non-zero rotations (c)

Matrix $\mathbf{M}_c$ has $2n_b$ rows and columns, however, for a given configuration some of the displacements are zero, and it is sufficient to consider only a submatrix of $\mathbf{M}_c$, and the corresponding subvectors of $\ddot{\boldsymbol{\varphi}}$ and $\mathbf{m}$.

In determining the response of the structure three tasks must be considered:

1) solving (a subset of) Eq.(6) for a given configuration *(3.3)*,
2) determining the opening of some of the interfaces *(3.2.2)*,
3) solving for closing of one of the interfaces *(3.2.3)*.

3.2.2 Model for opening

If at one (or more) interfaces the eccentricity of the normal forces reaches the width of the column, one or more interfaces split open. Accordingly, the configuration changes and the equation of motion (Eq.(6)) must be solved (see subsection 3.3) with this new geometry. In this section the procedure of finding the new open interfaces is discussed.

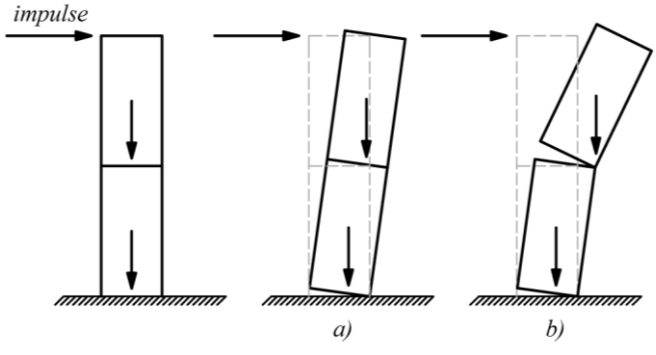

Fig. 18 False opening solution of a two-block column

It seems a good strategy either to open the interface where the eccentricity is the highest or to open all the interfaces where the eccentricities are outside the width of the blocks. We found, however, that this procedure might be numerically unstable. The reason that the change in the acceleration within one time step can be high enough to open more than one interfaces as is illustrated in Fig. 18, where two blocks are subjected to gravity loads and to a horizontal top impulse. It is assumed that the forces cause at both interfaces higher eccentricity than the block's width at both interfaces. Following the above strategy results in the configuration shown in Fig. 18b. If we solve the equation of motion with this configuration we receive impossible solution (Eq.(5)), since the sign of the opening at the bottom will be the opposite of that shown in Fig. 18b. In reality the opening scheme will be the one shown in Fig. 19e. In theory there are 8 possible opening configurations (see Fig. 19a-h), however, the one shown in Fig. 19e will occur. To overcome this difficulty there are two options: either (i) the length of the time step is reduced to ensure that the change in acceleration is small and there are several time steps between the opening of each interface or (ii) we consider all the kinematically admissible configurations.

If there are n_{closed} closed interfaces, the total number of possible cases is $(3^{n_{\text{closed}}} - 1)$, since every interface can open clockwise, counterclockwise or can remain closed, however, it is impossible that all the interfaces remain closed.

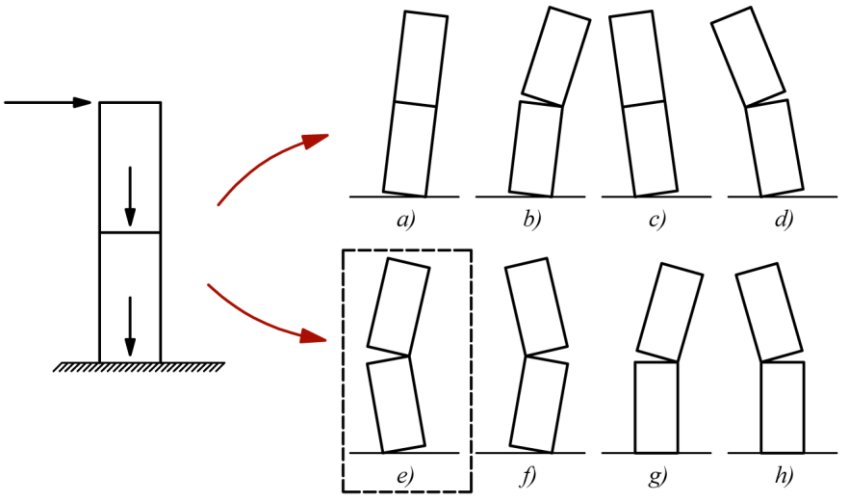

Fig. 19 Possible cases of a two-block column

When the number of closed interfaces (n_{closed}) are not high, $n_{\text{closed}} \leq 9$ (if $n_{\text{closed}} = 9$, the number of cases is about 20 000) the recommended strategy is as follows:

- determine all the possible cases $(3^{n_{\text{closed}}} - 1)$,
- chose those where the displacements after the first time step are compatible (see Eq.(5)), these are the kinematically admissible configurations,
- if there are more than one kinematically admissible configurations, chose the one where the kinetic energy is the highest. (Note that so far we have found always only one admissible configuration.)

When the number of the closed interfaces is high, the above procedure is very time consuming, and it is a better strategy to reduce the length of the time steps.

3.2.3 The impact model

When an interface (e.g. the i^{th} one) is closing impact occurs. First we discuss how the change in velocities can be calculated if the opening configuration after impact is assumed to be known. An example is shown in Fig. 20, where impact occurs at the third interface; the first interface remains closed after impact, while

the third and fourth one open up. The change in angular velocities is calculated according to Eq. (B6) (see Appendix B):

$$\begin{Bmatrix} \Delta v_1 \\ \vdots \\ \Delta v_{i-1} \\ \Delta v_{i+1} \\ \vdots \\ \Delta v_m \end{Bmatrix} = \begin{bmatrix} m_{1,1} & \dots & m_{1,\mathrm{i}-1} & m_{1,\mathrm{i}+1} & \dots & m_{1,\mathrm{m}} \\ \vdots & \ddots & \vdots & \vdots & \ddots & \vdots \\ m_{\mathrm{i}-1,1} & \dots & m_{\mathrm{i}-1,\mathrm{i}-1} & m_{\mathrm{i}-1,\mathrm{i}+1} & \dots & m_{\mathrm{i}-1,\mathrm{m}} \\ m_{\mathrm{i}+1,1} & \dots & m_{\mathrm{i}+1,\mathrm{i}-1} & m_{\mathrm{i}+1,\mathrm{i}+1} & \dots & m_{\mathrm{i}+1,\mathrm{m}} \\ \vdots & \ddots & \vdots & \vdots & \ddots & \vdots \\ m_{\mathrm{m},1} & \dots & m_{\mathrm{m},\mathrm{i}-1} & m_{\mathrm{m},\mathrm{i}+1} & \dots & m_{\mathrm{m},\mathrm{m}} \end{bmatrix}^{-1} \begin{Bmatrix} m_{1,i} \\ \vdots \\ m_{i-1,i} \\ m_{i+1,i} \\ \vdots \\ m_{m,i} \end{Bmatrix} \Delta v_i \tag{7}$$

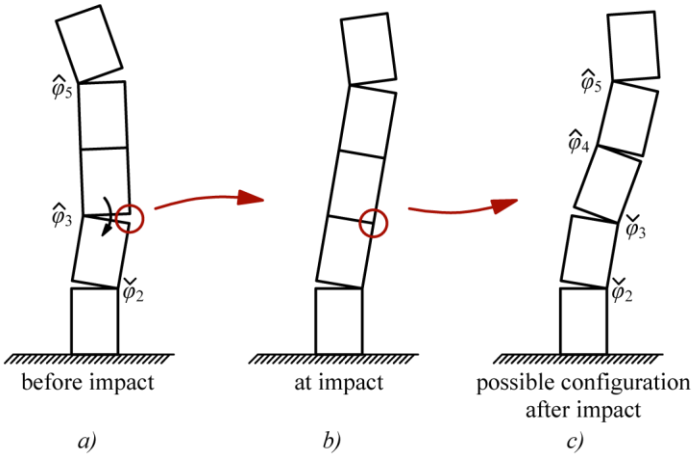

Fig. 20 Configuration before (a), during (b) and after (c) the impact

where Δv_i is the angular velocity of the closing interface before impact, $\Delta v_1 - \Delta v_\mathrm{m}$ are the change in velocities of the opening interfaces, and m_{ij} are the elements of the mass matrix. For the case shown in Fig. 20 Eq.(7) becomes:

$$\begin{Bmatrix} \Delta\dot{\hat{\varphi}}_2 \\ \dot{\check{\varphi}}_3 \\ \dot{\hat{\varphi}}_4 \\ \Delta\dot{\hat{\varphi}}_5 \end{Bmatrix} = \begin{bmatrix} m_{2,2} & m_{2,3} & m_{2,9} & m_{2,10} \\ m_{3,2} & m_{3,3} & m_{3,9} & m_{3,10} \\ m_{9,2} & m_{9,3} & m_{9,9} & m_{8,10} \\ m_{10,2} & m_{10,3} & m_{10,9} & m_{10,10} \end{bmatrix}^{-1} \begin{Bmatrix} m_{2,8} \\ m_{3,8} \\ m_{9,8} \\ m_{10,8} \end{Bmatrix} (-)\dot{\hat{\varphi}}_3. \tag{8}$$

Interfaces 3 and 4 open up, hence for these interfaces the changes in velocities are identical to the new velocities, while interfaces 2 and 5 are open before (and after) impact, for these interfaces Eq.(8) gives the change in angular velocities.

Now the kinematically admissible configurations are discussed. To choose the proper case is not an easy task, and it was found − similarly to the opening model − that in many cases the case, which seems trivial, is physically impossible. This is why we decided to investigate all the possible options.

Assume that there are n^{closed} closed interfaces before impact. Each can be closed or open clockwise or counterclockwise after impact. This means that the total number of cases is

$$2 \times 3^{n_{\mathrm{closed}}}, \tag{9}$$

where 2 is due to the fact that the closing interface (where the impact occurs) may either split open (opposite to the closing direction), or remain closed (see Fig. 16 and Fig. 21), however it is assumed that the impact is inelastic and the closing interface cannot bounce back. (For elastic impact bouncing back is a realistic option (Vassiliou et al. 2015; Giouvanidis and Dimitrakopoulos 2017)).

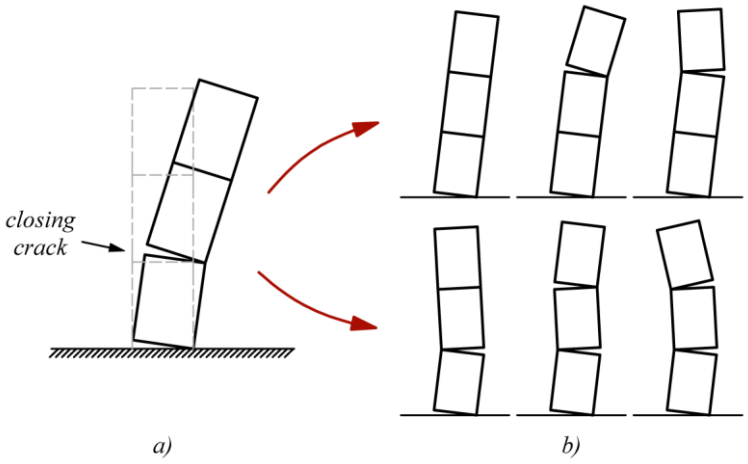

Fig. 21 The possible rocking motions after impact (n_{closed}=1)

The following strategy is recommended if n_{closed} is small

- for each case (Eq.(9)) determine the change in velocities during impact (Eq.(7)),
- throw out the kinematically impossible configurations, where at the opening interface $\dot{\varphi}_i \geq 0$, $\dot{\varphi}_i \leq 0$,
- if there are more than one kinematically admissible configuration chose the one for which the kinetic energy ($E_{kin} = \frac{1}{2}\dot{\boldsymbol{\varphi}}^T \mathbf{M}_c \dot{\boldsymbol{\varphi}}$) is the highest, i.e. where the dissipated energy is the lowest.

When the number of closed interfaces is high a search scheme should be developed, which is not implemented yet.

The impact model and Eq.(7) was verified by the expressions presented by Psycharis (1990) for a two block mechanism. Two blocks (height=300 mm, width=100 mm, m=15 kg) are placed on top of each other (Fig. 22a). The lower block is motionless, while the upper one rotates around its corner and reaches the interface by angular velocity $\omega_{2,before}$ =1.0 1/s (Fig. 22a). It is assumed that after impact both interfaces open up (Fig. 22b). The 4 by 4 mass matrix of the system is:

$$\mathbf{m} = \begin{bmatrix} 3.700 & 1.175 & 3.550 & 1.100 \\ 1.175 & 0.500 & 1.100 & 0.425 \\ 3.550 & 1.100 & 3.700 & 1.175 \\ 1.100 & 0.425 & 1.175 & 0.500 \end{bmatrix}, \tag{10}$$

while Eq.(7) gives

$$\begin{Bmatrix} \Delta\omega_1 \\ \Delta\omega_2 \end{Bmatrix} = \begin{bmatrix} 3.700 & 1.175 \\ 1.175 & 0.500 \end{bmatrix}^{-1} \begin{Bmatrix} 3.550 \\ 1.100 \end{Bmatrix} 1.0 = \begin{Bmatrix} 0.1079 \\ 0.5965 \end{Bmatrix} \left[1/s\right], \tag{11}$$

where $\Delta\omega_i$ is the change of the angular velocity in the i^{th} interface. Since both velocities are positive the opening is kinematically admissible (Eq.(5)). The angular velocities of the blocks are: $\omega_{block,1}$=0.1079 [1/s], $\omega_{block,2}$=0.7044 [1/s]. (The change in kinetic energy is 25.6%.)

The angular velocities were also calculated by Eq. 24 of Psycharis (1990), and we obtained the same results.

(If – instead of Housner's model – two consecutive impacts are assumed (see section 3.1), the velocities are: $\omega_{block,1}$=0.0539 [1/s], $\omega_{block,2}$=0.7443 [1/s], and the change in kinetic energy is 13.9%.)

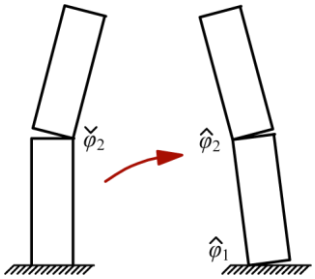

Fig. 22 A possible opening scheme of the investigated two-block system

3.3 Dynamical model for multi-block structures

Several robust methods are available to solve Eq.(6), here Wilson's method (Chopra 1995) is applied. Note that the size of the problem depends on the number of open interfaces, if n_h ($\leq n_b$) interfaces are open there are n_h unknowns. To start the calculation the initial displacements, $\boldsymbol{\varphi_0}$ and the initial velocities, $\dot{\boldsymbol{\varphi}}_{\mathbf{0}}$ must be given. (At the very first calculation both are zero.) At every time step three conditions were investigated:

- at every closed interface the eccentricity of the normal force must be within the width of the elements,
- at every open interface the motions must satisfy Eq.(5),
- at every interface the N normal force must be compression, and $\mu N \geq |V|$, where μ is the friction coefficient and V is the shear force.

If either one of these is not satisfied the calculation is terminated and in the first two cases the instant of termination is calculated by linear interpolation within the last step.

In the first case one (or more) closed interfaces must split open (see section 3.2.2), in the second case impact occurs (see section 3.2.3), while in the third case the column may disintegrate and the whole process is terminated. (After sliding at an interface the column may carry further loads, however, this case is not investigated in this thesis.)

When the termination is due to the first or second case, we recalculate (see section 3.2.2 and 3.2.3) the configuration (new geometry) and the initial velocities, and solve again the equation of motion (Eq.(6)).

The change in geometry was taken into account by recalculating the geometry at each time step. Numerical comparisons showed that this simple procedure – since in Wilson's method relatively small time steps are required – has high accuracy. (We compared the results for the cases, when the geometry was recalculated in every second and fourth time step. The results were practically identical.)

Calculation of a column

As long as the base excitation causes small eccentricities it is assumed that the column – as a rigid body – moves together with the base. When the eccentricity reaches the width of the elements first the "opening model" is executed, which is followed by Wilson's method with initially zero displacements and speeds. It is terminated if one of the conditions given in section 3.2 does not hold.

Following that either the opening or the impact model is executed, and then the equation of motion is solved again as described above. The calculation is terminated when tension or obvious failure (overturning) occurs.

3.4 Summary

It was found that the main reason for the difference between Housner's impact model and the experimental results is that in the original model the best case scenario was assumed: that impact occurs at the edges (Fig. 13b), which results in the maximum energy loss. In reality, due to the unevenness of the surfaces, or due to the presence of aggregates between the interfaces, rocking may occur with consecutive impacts, which reduce the energy loss.

A simple possible phenomenological improvement of Housner's model is that one additional bump (and consequently an additional impact) is assumed in the middle of the interface (Fig. 13c). This modified model is proposed to be taken into account, when masonry and stone columns and arches (Fig. 5) are analysed.

The most important new features of the multi-block model are the "opening" and the "impact" model. In both cases several new configurations (crack patterns) may occur, the right one is chosen by investigating the signs of motions and the change in kinetic energy.

In formulating the impact model the mass matrix must be formulated for the case where (at the interface where impact occurs) both the clockwise and counterclockwise openings are considered (Fig. 17b): this is also a new and necessary element of the model.

We emphasize that the model is purely mechanical: assuming rigid blocks and classical (inelastic) impact. There are no numerically set parameters, we do not use any "fudge-factor". (Instead of Housner's model two consecutive impacts are considered, as it is described section 3.1.)

The new opening and impact models can be implemented also in FE programs (e.g. OpenSees), which may enhance the applicability of the models significantly.

Chapter 4 Experimental verifications of the model

At the *Adolf Czakó Laboratory* of BME several experiments were run to verify the models presented in Chapter 3.

4.1 Energy dissipation of a single rigid block

Two granite blocks were manufactured with different aspect ratios, shown in Fig. 23. (At two adjacent edges approximately 5 × 5 mm triangular prisms were cut off.) The depth of the blocks was 300 mm to maintain the 2D rocking motion, since blocks with square cross sections, as it is reported by Zulli et al. (2012), may show 3D twisting motion. The rocking of each block was tested in 4 different configurations (Fig. 24a-d):

a) rocking on the surface, where the corners are cut off,
b) rocking on the same surface with a 2 mm diameter wire attached at the midpoint,
c) two wires attached at the opposite surface, where two wires attached 7 mm from the edges middle *(Our intention was to place the two wires at the same distance as the width between the cuts, i.e. ~5 mm from the edges, however there is a small difference.),*
d) an additional 4 mm diameter wire attached at the middle.

Note that the Young modulus of the steel is about 3-4 times bigger than that of the granite, hence the somewhat softer contact has only a minor effect. (Table 3, configuration c shows that the calculated, theoretical value of the energy loss – assuming inelastic impact – is 17.2%, while the measured value – due to the deformations and/or the slip is only a little bit higher: 19.5%.) Configuration *a* basically agrees with Housner's case with the slight modification that the axes of rotations are 5 mm from the edges of the blocks. The reduction in kinetic energy slightly changes as well, as discussed in the Appendix A (see Eqs.(2) and (A3)).

In case of configurations *b* and *d* two impacts occur during rocking; while in case of configuration *c* it is made sure that one impact occurs exactly at the chosen position defined by the wires close to the edges.

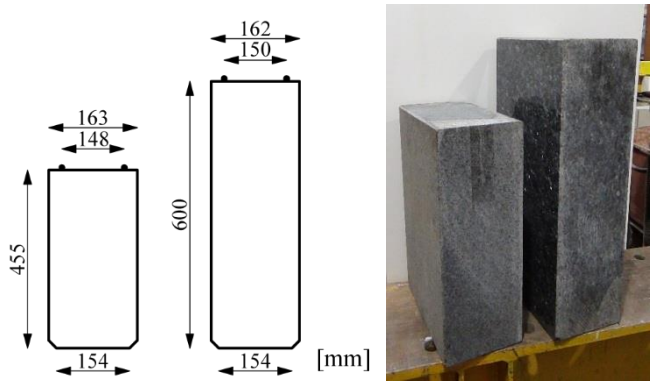

Fig. 23 Picture and the sizes of granite blocks used in the experiments

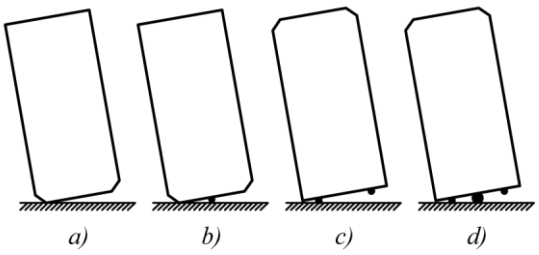

Fig. 24 Configurations of a block applied in the tests

We ran each configuration 40 times, hence, the number of performed tests is 320. In each test a block was placed on a horizontal, 35 mm thick steel plate, the block was tilted close to its neutral position, and then it was moved by the gravity force (free rocking). The motion was measured by an x-IMU device with 256 Hz accuracy. (For comparison, in a few cases one of the blocks were placed on top of the other granite block instead of the steel surface. The results of rocking were identical to those when rocking was performed on a steel plate.)

A typical displacement (angle of rotation) curve as a function of time is given in Fig. 25 by solid line.

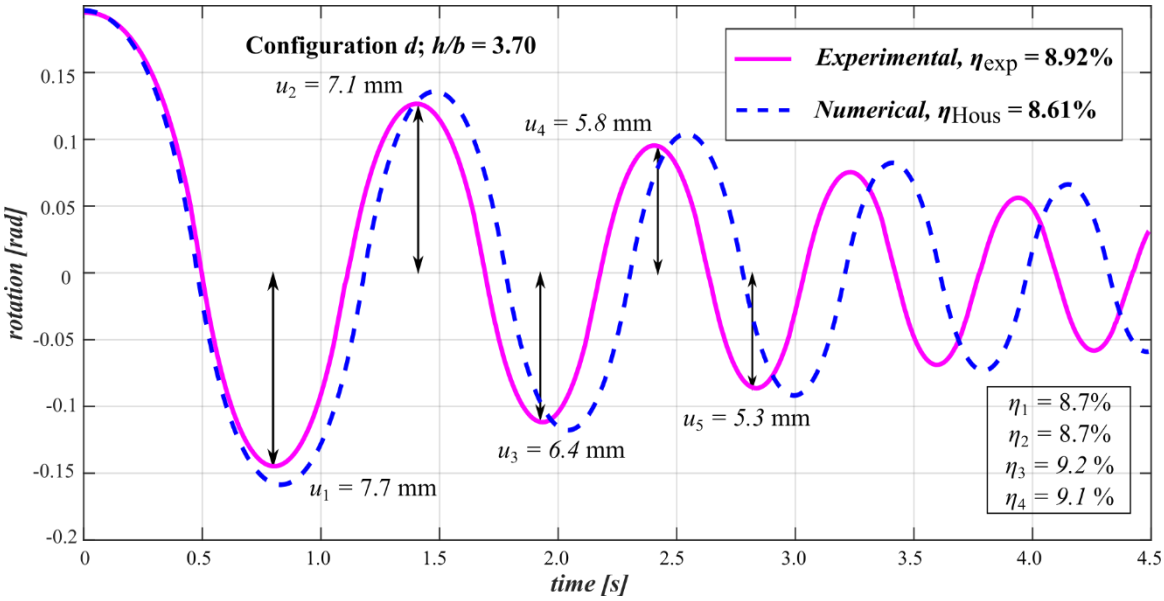

Fig. 25 Angle of rotation as a function of time, configuration d) (the potential energy of the block was measured at the maximum amplitudes of the rotations marked with arrows)

An important measure of the behaviour of the system is the change in kinetic energy before and after each rocking. The system has kinetic and potential energy. The first one is zero when the vertical displacement is maximum, while the second one is taken to be zero when the angular rotation is zero, and hence the vertical displacement is minimum. As a consequence, by neglecting the energy loss between two consecutive impacts, the maximum kinetic energy is identical to the maximum potential energy (E_i). Thus E_i can be calculated by multiplying the maximum vertical displacement of the centre of gravity by the weight of the block. The relative energy loss is calculated as

$$\bar{\eta}_i = \frac{E_i - E_{i+1}}{E_i} \approx \frac{u_i - u_{i+1}}{u_i}, \tag{12}$$

which is also shown in Fig. 25. In Eq.(12) u_i and u_{i+1} are the amplitudes of displacements before and after the i-th rocking. (We applied the "bar" to identify that $\bar{\eta}$ is obtained from an experiment.) It is important to notice that with reasonable accuracy the values of $\bar{\eta}_i$ are identical at every rocking. $\bar{\eta}$-s – calculated as the average of four consecutive $\bar{\eta}_i$-s of each experiments, are given in the first two columns of Table 2 and Table 3. The presented numbers are the average of 40 tests, which are followed ± the standard deviation. We may observe that the highest standard deviation belongs to configuration a, where the unevenness of the surface affects the impact.

During the impacts it was observed that small slips (and a minor twisting) occurred, which means that part of the loss in energy is due to the slips and not due to the impact. In two cases, identified in Table 3 by an asterisk, the slip was significant.

By comparing the experiments to each other a few important observations can be made.

Table 2 Relative energy loss between adjacent rockings in the experiments ($\bar{\eta}$) and in Housner's model (η_{HousC}, Eqs. (1), (2) and (A3))

		$\bar{\eta}$		η_{HousC}	
		Slenderness: h/b		*Slenderness: h/b*	
		2.79	3.70	2.79	3.70
configuration	*a*	13.4±3.0%	12.4±0.9%	28.4%	17.7%

Table 3 The relative energy loss between adjacent rockings in the experiments ($\bar{\eta}$) and in the calculation (η_{HousC} for configuration *c*, and $\eta_{\mathrm{HousC}}^{2\mathrm{imp}}$ for configuration *b* and *d*.)

		$\bar{\eta}$		η_{HousC} & $\eta_{\mathrm{HousC}}^{2\mathrm{imp}}$	
		Slenderness: h/b		*Slenderness: h/b*	
		2.79	3.70	2.79	3.70
configuration	*b*	11.2±1.2%	6.9±0.4%	14.8%	9.0%
	c	57.9%*	19.5±1.0%	26.5%	17.2%
	d	22.9%*	8.8±1.0%	13.8%	8.6%

1) $\bar{\eta}_{\mathrm{a}} < \eta_{\mathrm{HousC}}$, as it was expected the energy loss in the experiment is much smaller than in Housner's model (13.4<28.4; 12.4<17.7; Table 2).
2) $\bar{\eta}_{\mathrm{a}} < \bar{\eta}_{\mathrm{c}}$, i.e. when impacts are enforced to occur at the edge, the energy loss is higher than on the rocking block (12.4<19.5; Table 2 and Table 3). Note that significant slips occurred with configuration *c* for the lower aspect ratio during the motion, which explains the very high energy loss.
3) $\bar{\eta}_{\mathrm{b}} < \bar{\eta}_{\mathrm{c}}$, the energy loss is smaller if two impacts occurs instead of one (11.2<57.9; 6.9<19.5; Table 3).
4) $\bar{\eta}_{\mathrm{c}} \simeq \bar{\eta}_{\mathrm{HousC}}$, if it is made sure that impact really occurs at the edges the difference between the experiments and Housner's model is small at the slender block (19.5>17.2; Table 2 and 3).
5) $\bar{\eta}_{\mathrm{a}} > \bar{\eta}_{\mathrm{b}}$, an enforced impact at the middle decreases the loss in energy, note, however, that the difference is much smaller than in item 1 (11.2<13.4<28.4; 6.9<12.4<17.7; Table 2 and 3).

We can also extended Housner's rocking model with the following modifications:

- impact may occur at an arbitrary position, not only at the corners. The equations corresponding to this modification are given in Appendix A.
- several impacts may arise consecutively (see Appendix A for two consecutive impacts).

With these modifications the motion of the blocks with configurations *b*, *c* and *d* were also calculated. A typical example is shown in Fig. 26. The relative loss in energy is given in the last two columns of Table 3. In every case the experimental values are 1-3% off the calculated value. That difference is much smaller than between the "classical" experiments (configuration *a*) and Housner's model (5-15%, see

Table 2). For configurations *b* and *c* the change in the amplitudes in the experiments and the calculations are close to each other (Fig. 26b, c), while for configuration *a* the original Housner's model overpredicts the change in amplitude, and the modified underpredicts it (Fig. 26a).

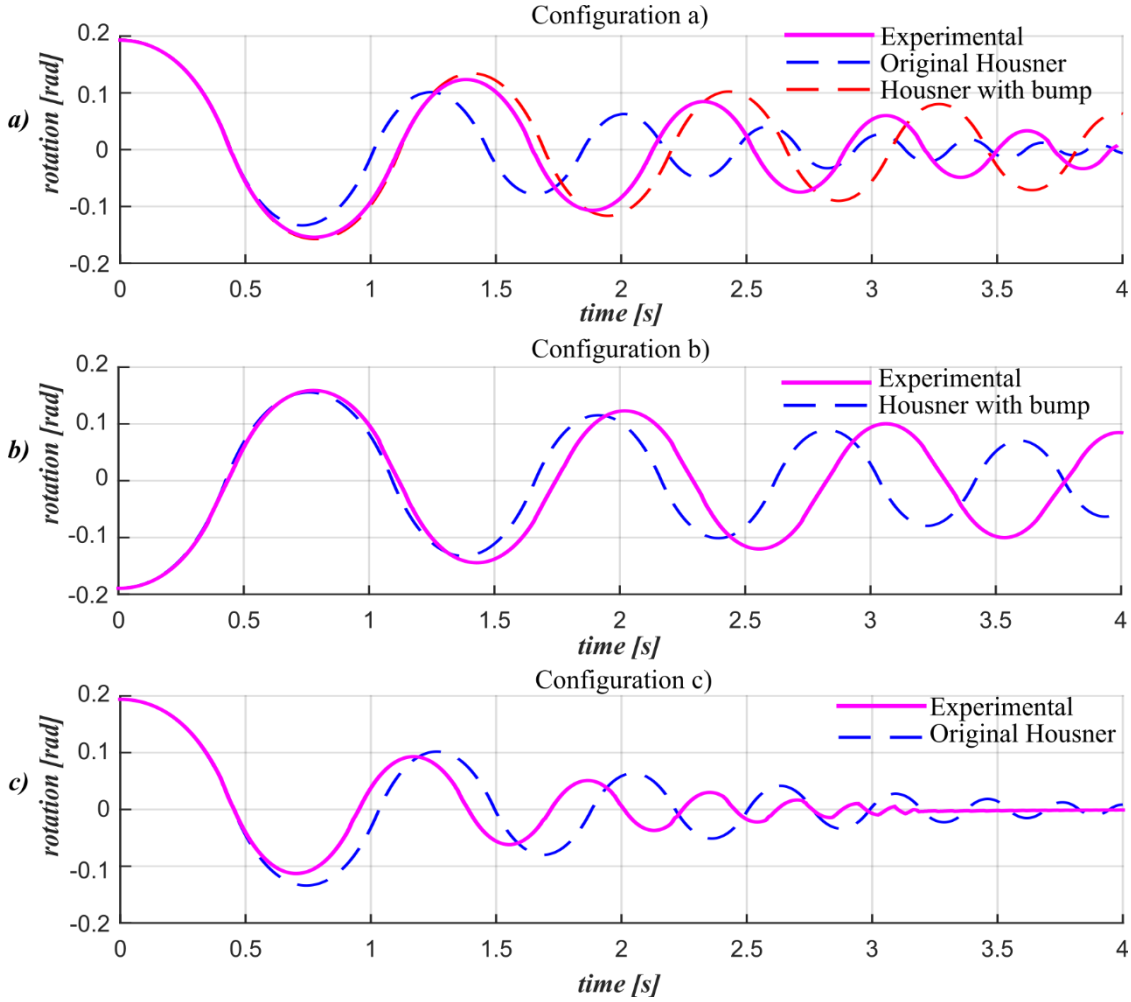

Fig. 26 Examples of the experimental results for configuration a), b) and c), investigating the block with slenderness 3.7

It is also an important observation that $\bar{\eta}_a > \bar{\eta}_b$, however, the difference is smaller than the difference between $\bar{\eta}_a$ and the classical Housner's model. It seems a reasonable approximation for the modeling of a rocking block that a bump is assumed at the middle of the block. According to our calculations and experiments this is a conservative approximation since this model underpredicts the loss of energy (while the classical Housner's model overpredicts it).

We have also tested this hypothesis with the experiments published by Ogawa (1977); Aslam et al. (1980); Prieto-Castrillo (2007) and Elgawady et al. (2011). See Fig. 27, where the dashed line represents Housner's model with an extra bump in the middle.

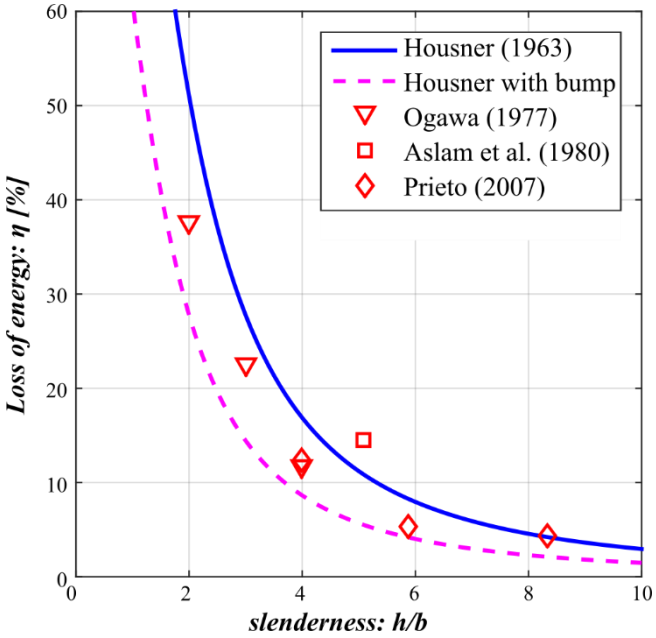

Fig. 27 Experimental results compared with the classical Housner's model and with the refined model including a bump in the middle.

4.2 Opening schemes of multi-block structures

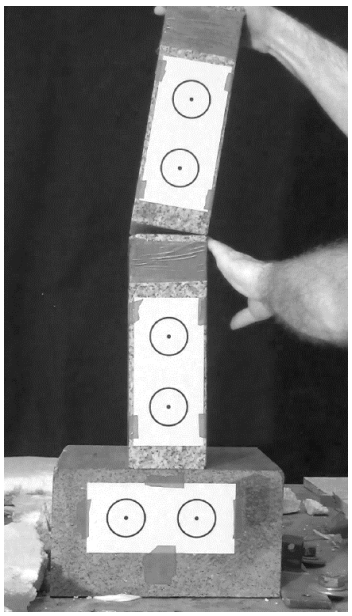

Fig. 28 The initial inclination of the two-block system

Two granite blocks (height=300 mm, width=100 mm, thickness=200 mm) were placed on top of each other (Fig. 28). The edges of the blocks were cut off, so the connected width of the elements were 96 mm. The upper block was released from an inclined position (φ_2=0.153 [rad]) and the rotation of the blocks was measured by x-IMU devices with 256 Hz sampling rate. The recorded and the simulated rotations of the blocks are presented in Fig. 29. As it was mentioned before (Section 3.1), the energy loss during impact is lower than the one predicted by Housner's model which can be taken into account by assuming two consecutive impacts (Ther and Kollár 2017d) (see Fig. 11a).

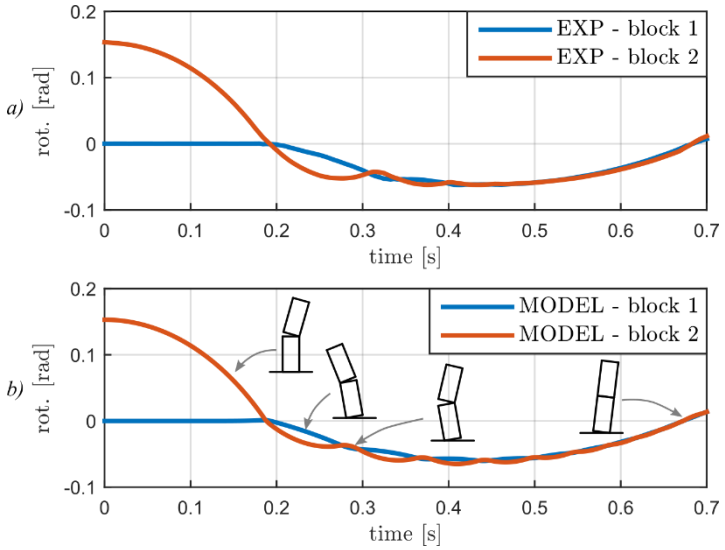

Fig. 29 The recorded (a) and the simulated (b) rotations of the two-block system during the free-rocking experiments

According to our calculation at t=0.13 the lower interface also opens up slightly and the lower block rotates clockwise. The upper block impacts the lower at 0.187 s and rotates counterclockwise. The lower

block impacts the base at 0.193, and then it also rotates counter clockwise. Afterwards the upper element rocks on top of the lower one, and then the two blocks move together.

The measured and the calculated rotations are close to each other. More importantly the observed and predicted opening-configurations are practically identical. (An even better agreement can be reached if we take into account that the faces of the blocks are not perfectly perpendicular to each other. In the calculation perfect elements were assumed.)

4.3 Base excitation of multi-block columns

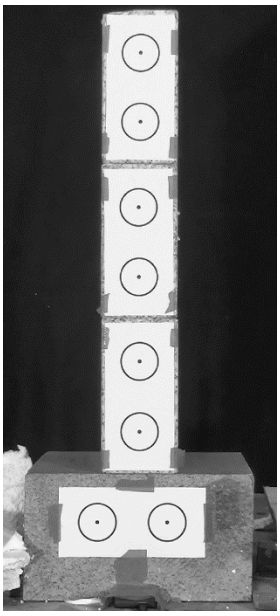

Fig. 30 The three-block column made of granite blocks

A column made of 3 granite blocks was investigated (Fig. 30). The dimension of the elements are height=200 mm, width=100 mm and the thickness is 300mm. The edges of the blocks (2x2 mm) were cut off.

The system was placed on a shaking table and it was excited by a motion shown in Fig. 31. (It is close to a sine pulse with period 0.6 s, and amplitude 45 mm.) The motions of the blocks and the shaking table have been recorded by a Full HD camcorder, with 50 frames per sec. The acceleration of the shaking table was also recorded by an x-IMU device. The rotations of the elements have been identified by an image-procession algorithm, written by the authors. One of the experimental results is presented in Fig. 32a.

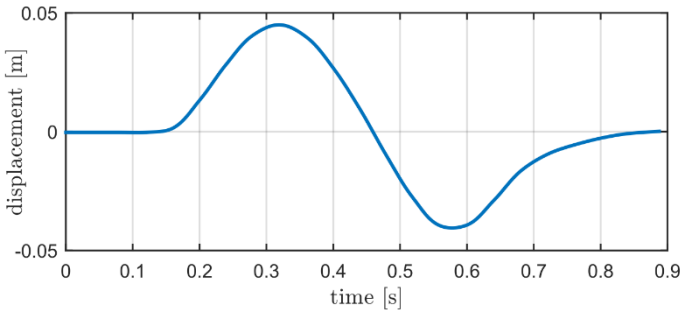

Fig. 31 The base excitation of the blocks (measured on the shaking table)

In Fig. 32b the calculated rotations of the three-block system is plotted. The measured base accelerations were used as input data for the calculations. The same opening and closing configurations are clearly visible. The experimental and the numerical results show acceptable agreement.

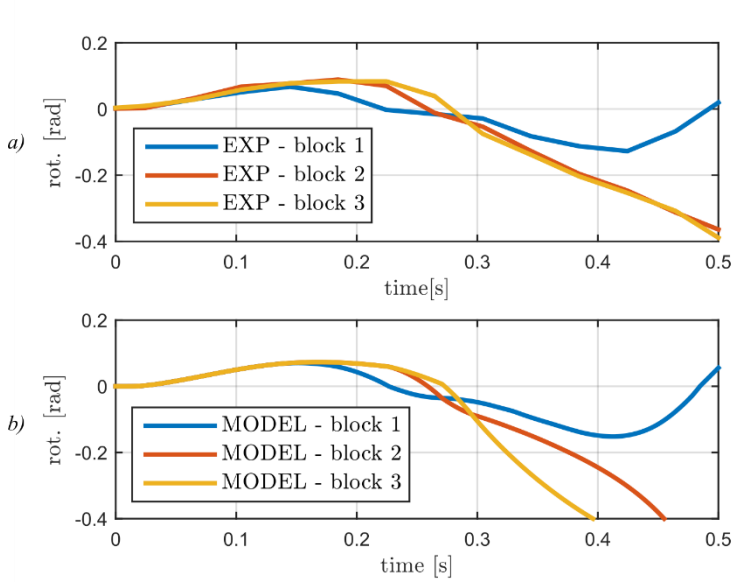

Fig. 32 The experimental (a) and numerical (b) results of a base excitation test

Chapter 5 Overturning of columns for base excitation

In the next subsections the overturning of single and multi-block structures are investigated. Overturning curves (OC) for simple signals are given in Fig. 8.

5.1 Overturning of single blocks for base excitation

5.1.1 Overturning Acceleration Spectra of single blocks for simple pulses

First, the *normalized overturning curve* (OC) (Housner 1963) is shown for a block with a given aspect ratio subjected to a single half sine pulse in Fig. 33a. Both axes are dimensionless, the vertical axis is normalized by $a_{p,min}$ (Eq.(3)), while the horizontal axis by the inverse of the "frequency parameter" (p), defined by Housner (1963):

$$p = \sqrt{\frac{mRg}{\Theta}} = \sqrt{\frac{g}{\alpha R}}, \quad \alpha = \frac{4}{3}, \tag{13}$$

where Θ is the mass moment of inertia about the corner point where the rotation occurs (Fig. 7), m is the total mass, R is the distance between the centre of mass and the corner point and g is the acceleration of gravity. Note that some researchers present acceleration as a function of pt_p (Yim et al. 1980; Voyagaki et al. 2013a) (as shown in Fig. 33), while others use its inverse, $1/(t_p p)$ (Zhang and Makris 2001; Makris and Konstantinidis 2003; Makris and Vassiliou 2012; Dimitrakopoulos and DeJong 2012; Dimitrakopoulos and Fung 2016).

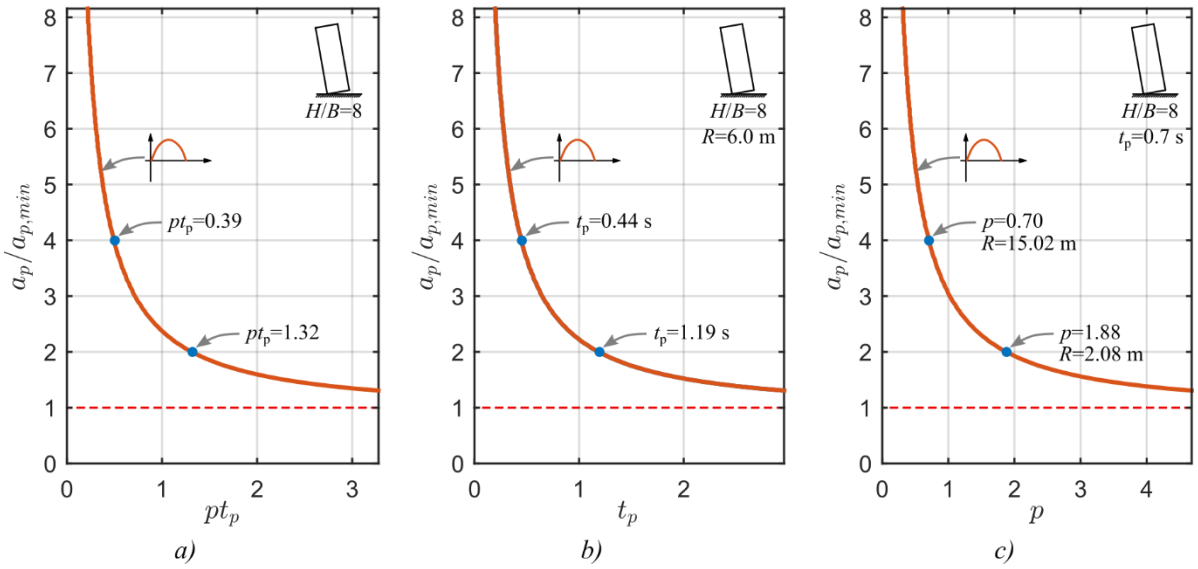

Fig. 33 Normalized overturning curve (OC) for a single block subjected to a half sine pulse (a) (see Housner (1963)). The OC shows the effect of the pulse length (b) while the OAS shows the effect of the block size (c).

The horizontal axis of Fig. 33a depends both on pulse duration and on block size. For a given block size (R=6.0 m in Fig. 33b) the OC is a function of the pulse length, while for a given pulse duration (t_p=0.7 s in Fig. 33c) it is a function of p. Hence the curve clearly shows a size effect. The smaller the block the more vulnerable it is to overturning.

The period of vibration T of a rocking block is defined as four times the duration between an inclined (motionless) φ_o position and the position of impact (φ=0). T depends on the block's maximum inclination (φ_o). Housner (1963) derived an approximate expression for T:

$$T \approx 4\sqrt{\frac{\alpha R}{g}}\cosh^{-1}\frac{\delta}{\varphi_o - \delta}. \tag{14}$$

Eq. (14) tends to infinity as φ_o approaches the neutral position δ of the block (Fig. 7). It can be shown that for a given inclination, φ_o the period of vibration is proportional to the square root of the block size:

$$T \sim \frac{1}{p} = \sqrt{\frac{\alpha R}{g}}, \quad \text{(for given } \varphi_0\text{)}. \tag{15}$$

Accordingly, on the horizontal axis of OAS we have the frequency parameter, which is proportional to the inverse of the period of vibration of the rocking block.

The plot in Fig. 33c is called *Overturning Acceleration Specra* (OAS), where the horizontal axis depends only on the block's size and not on the pulse duration. This representation will be used for earthquake records.

5.1.2 Overturning Impulse Curve

We define the impulse (I) and the fullness (F) of a single-lobe pulse in the following way:

$$I = \int_0^{t_p} a\, dt, \quad F = \frac{I}{a_p t_p}, \tag{16}$$

where a is the acceleration, t_p is the duration of the pulse and a_p is its maximum intensity (see Fig. 6a).

Either a longer duration or a higher impulse may cause the failure of a block. The horizontal coordinate of the *overturning curve* (Fig. 33a) is multiplied by Fa_p. By so doing we obtain the *overturning impulse curve* (Ther and Kollár 2017c), where on the horizontal axis we have the impulse: $Fa_pt_p=I$. Its normalized version is shown in Fig. 34b.

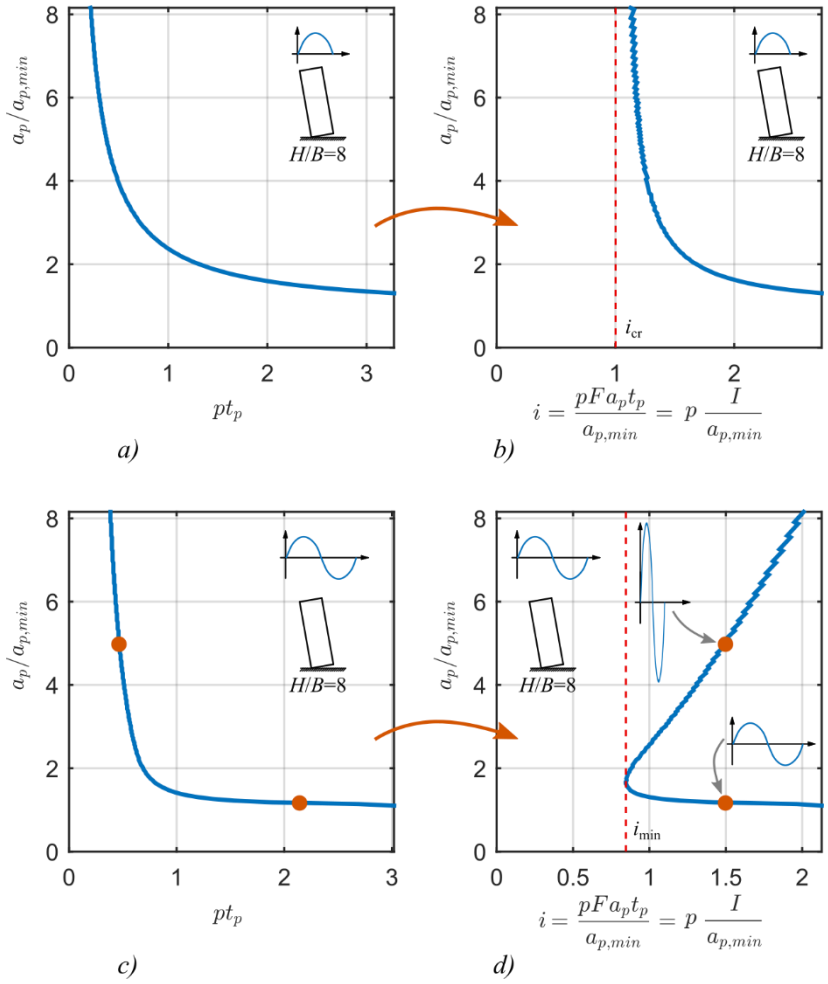

Fig. 34 The overturning curve and the overturning impulse curve for half (a,b) and full (c,d) sine pulses

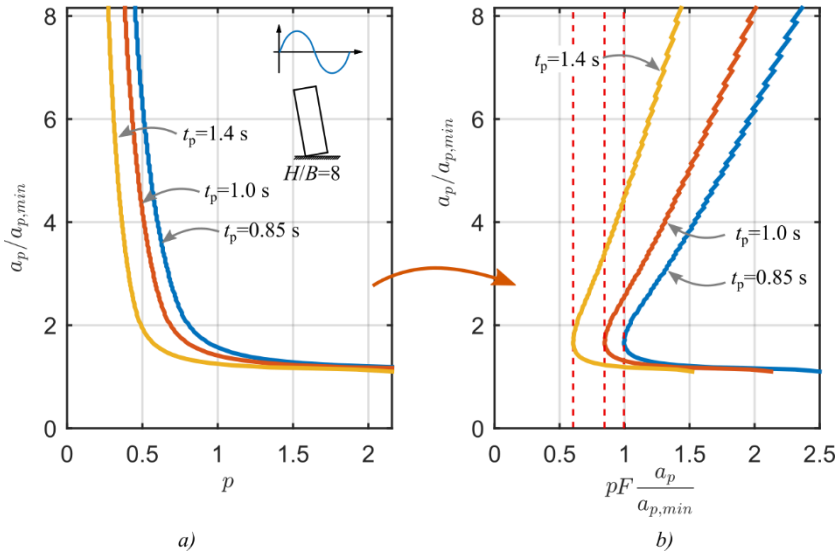

Fig. 35 The OAS (a) and the transformed OAS (b) of a full-cycle sine with different impulse durations

When there is a single-lobe pulse, the *impulse curve* is monotonic and tends to $pI_{\mathrm{cr}}/a_{p,min}$ (Fig. 34b), where I_{cr} is the critical impulse of a single-lobe pulse (where the duration tends to zero), which may cause the overturning of the block. Its value can be obtained from the elementary dynamics of a block (Ishiyama 1982; Makris and Vassiliou 2012):

$$I_{\mathrm{cr}} = \frac{1}{\cos\delta}\sqrt{2\alpha R g(1-\cos\delta)} \tag{17}$$

and the normalized critical impulse is defined as

$$i_{\mathrm{cr}} = p\frac{I_{\mathrm{cr}}}{a_{p,\mathrm{min}}} = \sqrt{\frac{2}{1+\cos\delta}} \geq 1. \tag{18}$$

The second equality was obtained from Eqs. (3) and (17). (For slenderness $H/B=\cot\delta=3$: $i_{\mathrm{cr}}=1.013$, while for $\cot\delta=8$: $i_{\mathrm{cr}}=1.002$, hence for an aspect ratio over 3: $i_{\mathrm{cr}}\approx 1$ is a reasonable approximation.)

When there are two (or more) pulses the *overturning impulse curves* are not monotonic, but there is a minimum value of the impulse (i_{min}), see Fig. 34d.

For a given duration (t_{p}), similar curves are shown in Fig. 35. The curves of Fig. 35a are the OAS for given simple signals, while the curves on Fig. 35b are obtained by the following transformation: the horizontal coordinate of the OAS is multiplied by $Fa_{\mathrm{p}}/a_{\mathrm{p,min}}$.

The overturning impulse curve (or the transformed OAS) contain the same information as the OC (or OAS). The advantage of their usage – as will be shown in section 5.3 – that it can be approximated by very simple functions; both for simple signals and for earthquake records.

5.1.3 Overturning acceleration spectra of single blocks for earthquake excitation

We define the *Overturning Acceleration Spectrum* (OAS) for an earthquake record (Ther and Kollár 2017c) as the curve which separates the safe and unsafe areas in the $a_p/a_{p,min}$, p coordinate system, where a_p is the maximum value of the ground acceleration, $a_{p,min}$ is given by Eq.(3), p is the frequency parameter given by Eq. (13). (Note that the size of the element and the intensity of the earthquake, i.e. the ground acceleration is scaled, but the frequency content of the earthquake is not modified.) An example is shown in Fig. 36a. The complexity of the earthquake record leads to several safe "bays" and "islands" within the unsafe region. We may observe, however, that the shape of the envelope is similar to those of simple signals. (This curve can be considered as the generalization of the curve suggested by Makris and Vassiliou (2012)). The dimension of the horizontal axis is 1/sec.

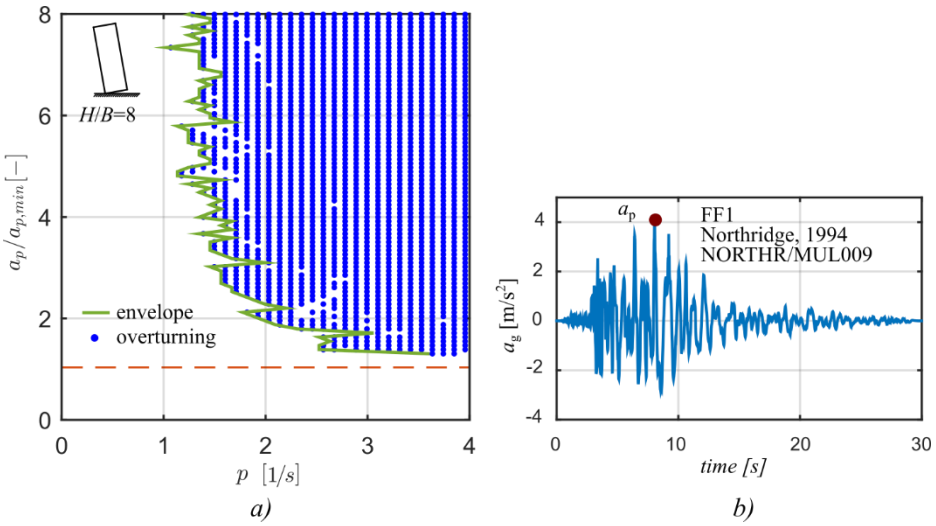

Fig. 36 The *Overturning Acceleration Spectrum* (OAS) of a single block (dot represents overturning) (a) based on the FF-1 earthquake record (Northridge-1994, NORTHR/MUL009 component) (b)

Analogously to the *overturning impulse curve* we defined the *transformed OAS* in such a way that the horizontal coordinate of the OAS (Fig. 37a) is multiplied by $a_p/a_{p,min}$. The result for an earthquake record is shown in Fig. 37b, where

$$f = p\frac{a_p}{a_{p,\min}}. \tag{19}$$

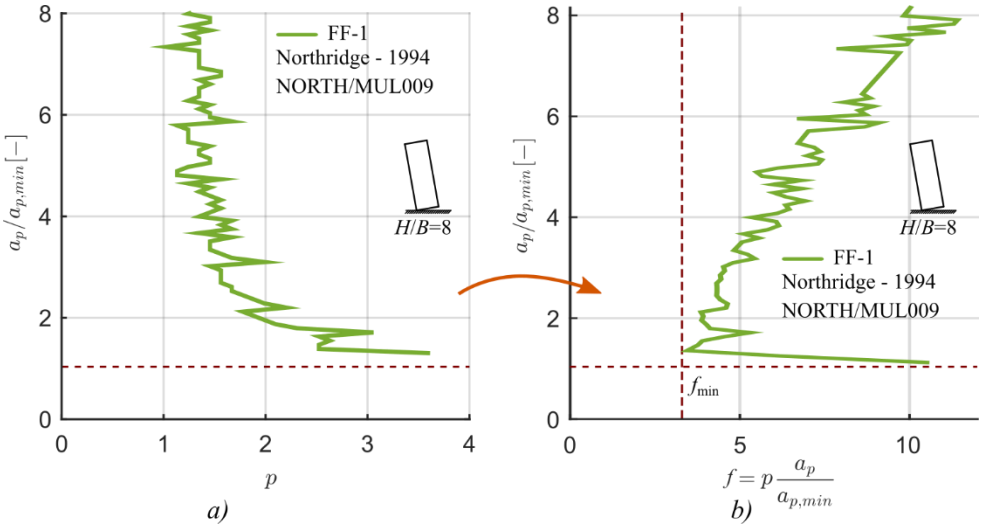

Fig. 37 The OAS (a) and the transformed OAS (b) for an earthquake record (Northridge – 1994, North/MUL009 component)

5.2 Overturning acceleration spectra of multi-block columns

The normalized *overturning curve* (OC) and *overturning acceleration spectra* (OAS) show the vulnerability of single blocks (Fig. 38a) to simple signals or earthquakes (see the previous sections). Two examples are shown in Fig. 39, one for a full sine pulse, the other for an earthquake record. The presented curves separate the unsafe and safe regions, i.e. where overturning occurs or can be avoided. The vertical coordinate depends on the maximum acceleration while the horizontal axis on the block size. (The horizontal axis of the normalized OC also depends on the pulse duration. p is the frequency parameter, defined by Housner (1963).)

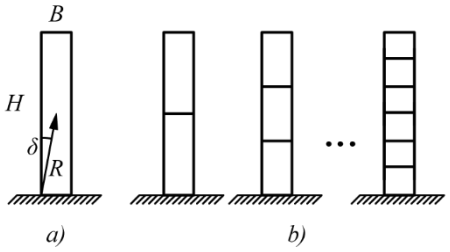

Fig. 38 The dimensions of a single block (a) and multi-block columns (b)

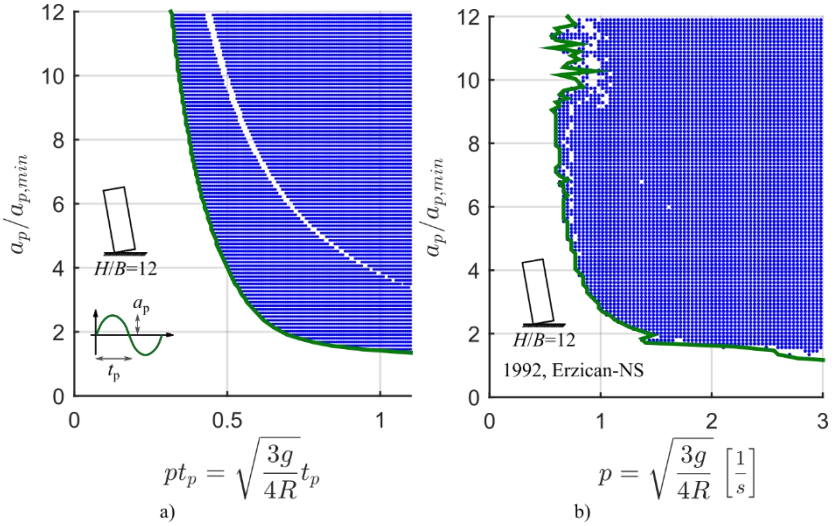

Fig. 39 The normalized overturning curve (OC) and overturning acceleration spectrum (OAS) of a single block of aspect ratio H/B=12 ($a_{\mathrm{p,min}} = \frac{B}{H}g$, $R = \frac{1}{2}\sqrt{H^2 + B^2}$). On the left the block was excited by a full sine pulse, on the right, by the 1992, Erzican - NS earthquake record

Now we investigate columns with the same aspect ratio (*H/B*) as those presented in Fig. 39, but the columns contain 2 and 3 blocks (Fig. 38b) (Ther and Kollár 2017b). The results are shown in Fig. 40 for *H*=12 m, *B*=1 m. In the plots the overturning of the structures are plotted on the a_p-t_p plane. It can be seen that with reasonable accuracy single blocks are more vulnerable than multi-block columns. For four cases, identified by green (safe) and red (overturning) stars in Fig. 40c, the full rotation-time curves are given in Fig. 42, for the three-block column.

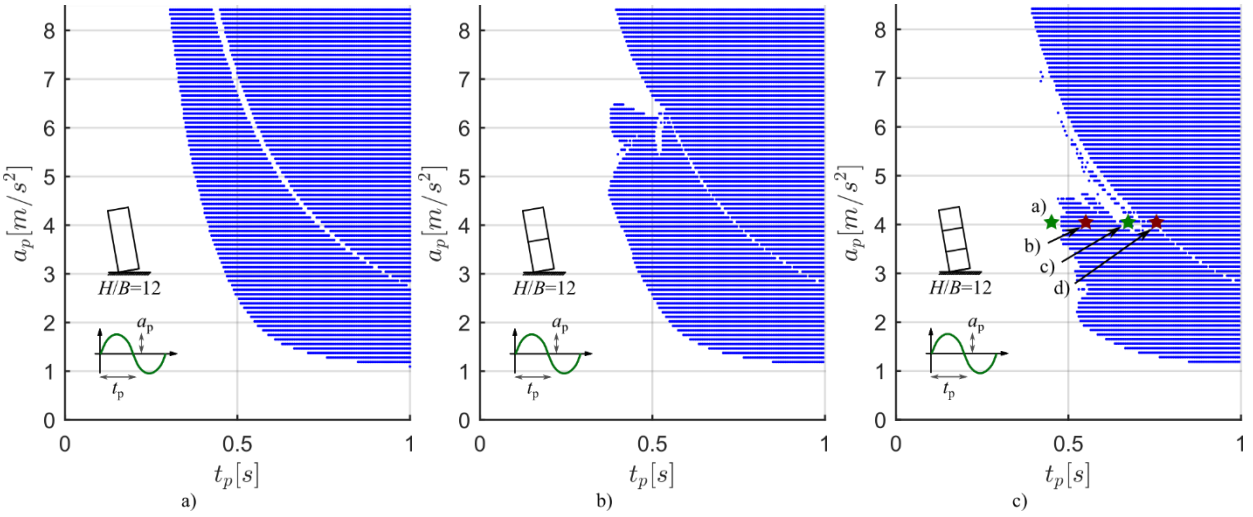

Fig. 40 The overturning of columns (H=12 m, B=1 m) consisting of 1, 2 and 3 blocks subjected to full sine pulse using Housner' model. The blue dots represent the unsafe solutions (overturning). In the third plot (c), the motions of the structure at the marked points are presented in Fig. 42.

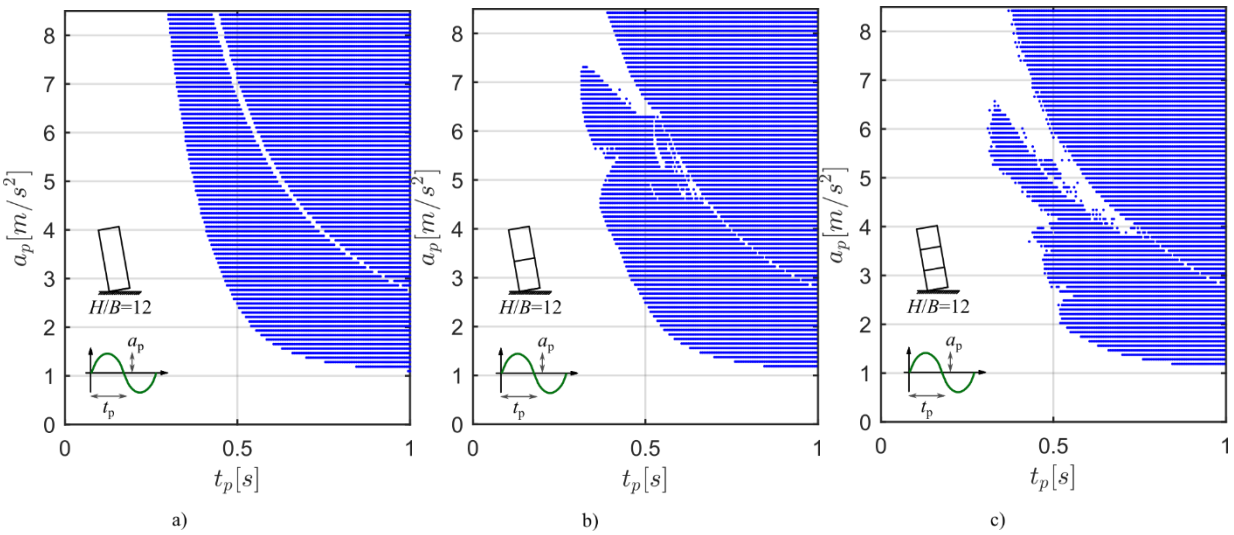

Fig. 41 The overturning of columns (H=12 m, B=1 m) consisting of 1, 2 and 3 blocks subjected to full sine pulse when there is no energy dissipation during impact.

We think that there are two reasons, why a multi-block system is safer than a monolithic:

- the effect of "higher mode" of the structure reduces the earthquake load;
- in higher modes the energy dissipation is also higher.

For curiosity the same structure was investigated, however assuming "rolling", no energy dissipation during impact. The results (Fig. 41) clearly show that with reasonable accuracy monolithic blocks are more vulnerable than multi-block structures. Note, however, that the difference is much smaller than in case of inelastic impact.

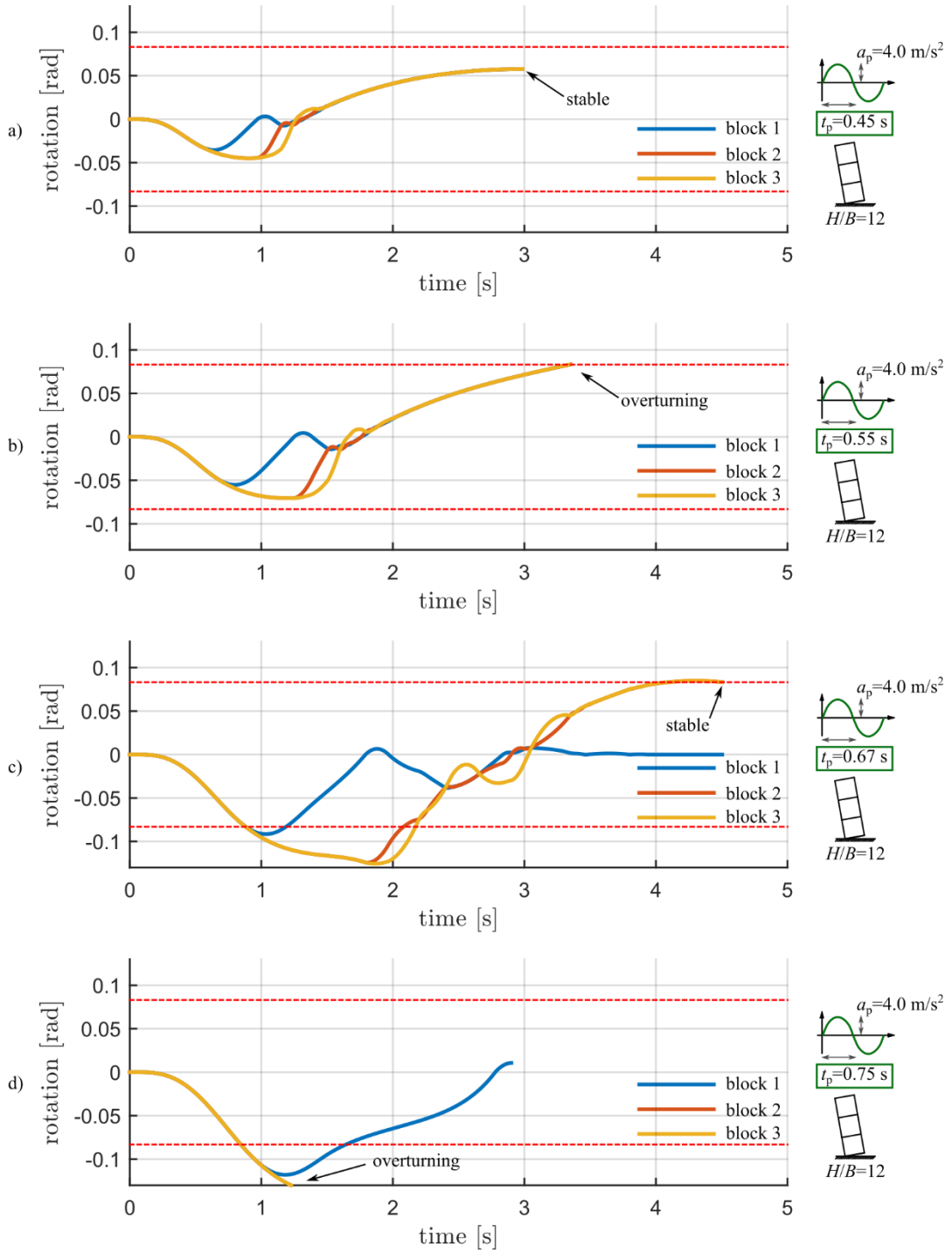

Fig. 42 Rotations of a three-block column excited by sine pulse with ap=4.0 m/s2 and with different tp. See Fig. 40c. The red dashed line represents the critical inclination of the column ($|\varphi_{crit}| = \delta$).

The effect of energy dissipation is shown in Fig. 43 for earthquake excitation. Three cases are presented:

1) 1 impact, which is identical to Housner's model (Fig. 13b),
2) 2 consecutive impacts, which is the recommended model (Ther and Kollár 2017d), and which agrees well – for a single block – with the experiments (Fig. 13c),
3) 10 consecutive impacts, when there is practically no energy dissipation, the elements 'roll' on each other (Fig. 12).

Note that the 1, 2 or 10 impacts are instantaneous, the total duration is zero.

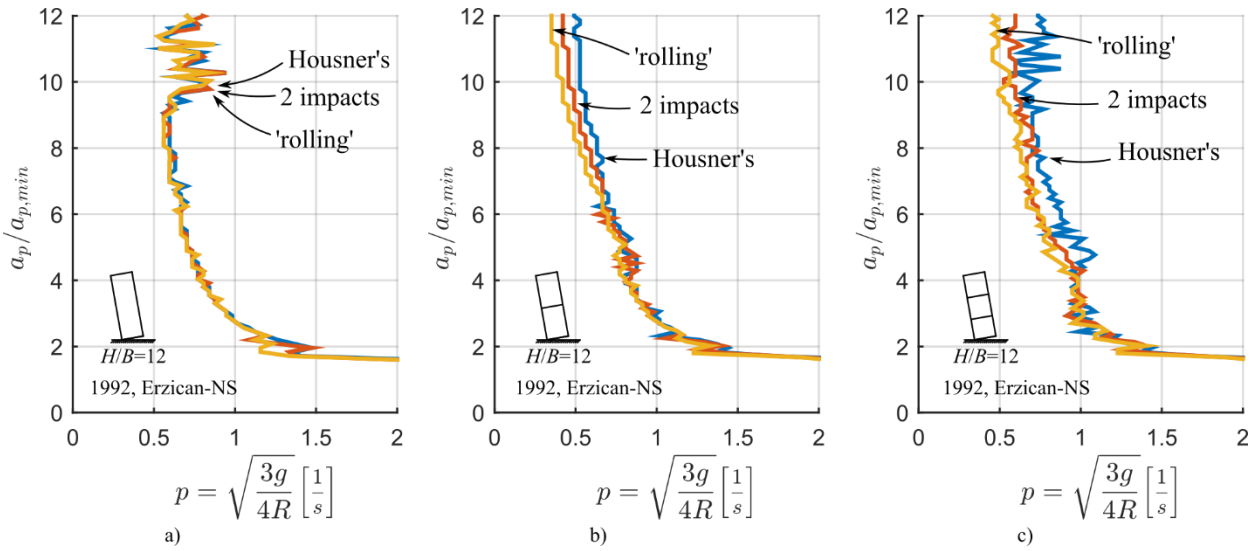

Fig. 43 The OAS of columns consisting of 1, 2 and 3 blocks with different energy dissipations. The column is subjected to 1992, Erzican-NS earthquake record.

As a rule the lower the energy dissipation, the more vulnerable structures are to overturning.

We may observe that the more the number of blocks in a column the more important the effect of energy dissipation is. The explanation is that during rocking the energy dissipations of a stocky element is higher than that of a slender one (Housner 1963). It is also clear that the effect of energy dissipation is more important for earthquake records than for simple signals, the reason is that there are more impacts for a complex record than for a simple pulse.

5.3 Design method for estimating the safety of rocking structures

We investigate the behavior of single rigid blocks, for it was shown, that single (monolithic) columns are more vulnerable, than multi-block columns (see section 5.2).

To obtain a design procedure for the investigation of a rocking block the approaches available in the literature are listed in Chapter 1 (page 5). Here a *new approach* is presented, which is based on the *Overturning Acceleration Spectrum* (OAS) defined in section 5.1.1.

After discussing this approach we present its simplified form: the *simplified* OAS.

The applicability of the approach was investigated numerically using time history analysis. In our research 56 near field (NF) and 44 far field (FF) records were considered (see Table 4 and Table 5), which are given in FEMA P695 (2009). We investigated 4 different aspect ratios (H/B=3, 5, 8 and 12), 80 different peak ground acceleration levels (from $a_{p,min}$ to 10 times $a_{p,min}$) and up to 120 different sizes (from R_{max}=1000 m down to R_{min}=0.1 m, always searching for the largest unsafe block size for a given peak ground acceleration).

In the numerical calculation Wilson's method is applied as described in Chapter 3. The impact is assumed to be inelastic, as it is stated in Housner's impact model (Housner 1963).

5.3.1 Characteristic Overturning Acceleration Spectra

For a given location we can determine the OAS for several earthquake records (Fig. 44a) and then a statistically determined *characteristic OAS* for a given probability of exceedance can be defined (Fig. 44b). The determination of this *characteristic OAS* is not the subject of our research, we just give a theoretical curve in Fig. 44b. In accordance with Housner (1963) we found numerically that block slenderness (considering monolithic column) has only minor effect on the OAS (Fig. 45), and the curve corresponding to higher slenderness is a safe approximation of the one which belongs to a lower slenderness. In the following calculation a reasonably high slenderness: H/B=12 will be used. As a consequence, the resulting *characteristic OAS* can be used for a wide range of aspect ratios.

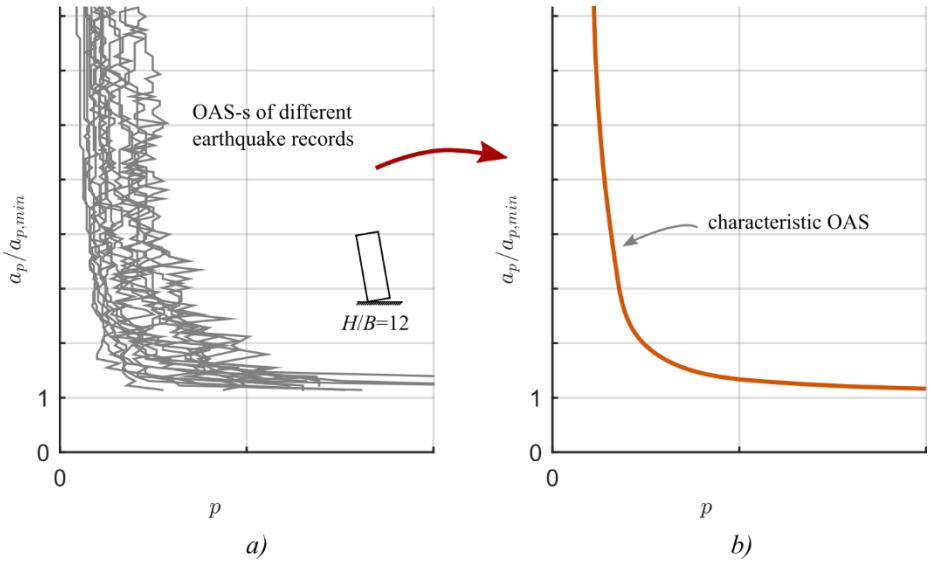

Fig. 44 OAS-s at a given location (a) and the determined *characteristic OAS* (b)

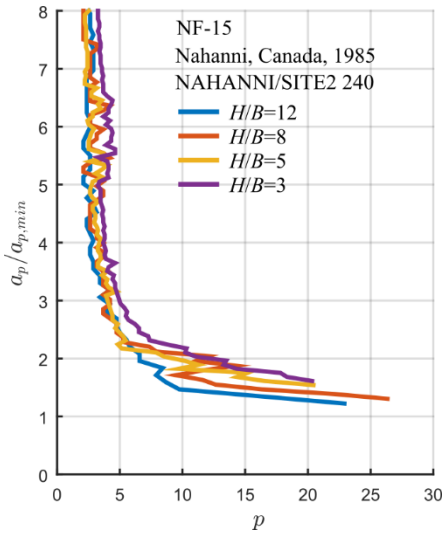

Fig. 45 The effect of block slenderness on OAS

5.3.2 Simplified Overturning Acceleration Spectra

Our aim is to have an OAS which can be represented by a few parameters. To reach this goal we consider the *transformed OAS* (Fig. 37b). In Fig. 46 transformed OAS are presented for simple signals. As we stated before for a single-lobe pulse the *overturning impulse curve* is monotonic (Fig. 34b), and hence the *transformed OAS* is also monotonic (Fig. 46a). When there is more than one pulse the *transformed OAS* becomes more complex. However, a vertical dashed line, shown in Fig. 46b-d can be used as an envelope in all cases. For the single pulse the ordinate of the asymptote is $\frac{i_{cr}}{Ft_p} = \frac{i_{cr}\pi}{2t_p}$. If t_p=0.5 s, the asymptote is at $\frac{i_{cr}}{0.32}\left[\frac{1}{s}\right]$. The location of the dashed lines for the other three cases are determined numerically.

For real earthquake records in most cases a vertical line at f_{min} is considered to be a reasonable approximation, which is shown in Fig. 47b. Note that for higher a_p-s *transformed OAS* diverges from the vertical line, and hence it might be argued that a better *simplified transformed OAS* can be obtained by one vertical and one inclined straight line (see section 5.3.5). Nevertheless, the single vertical line is definitely a safe and simple approximation, and hence it is the recommended approach.

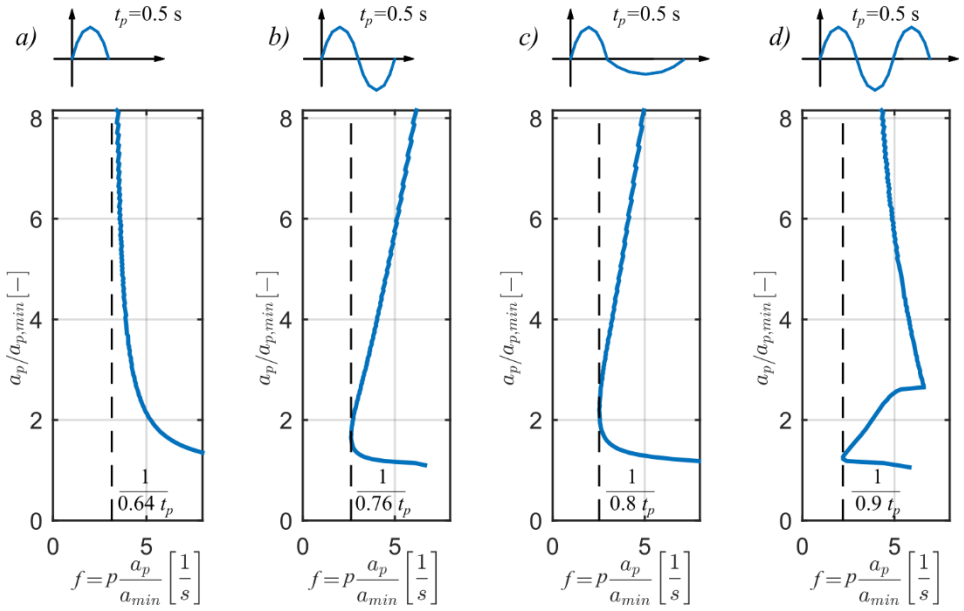

Fig. 46 The transformed OAS for simple signals (t_p=0.5 s)

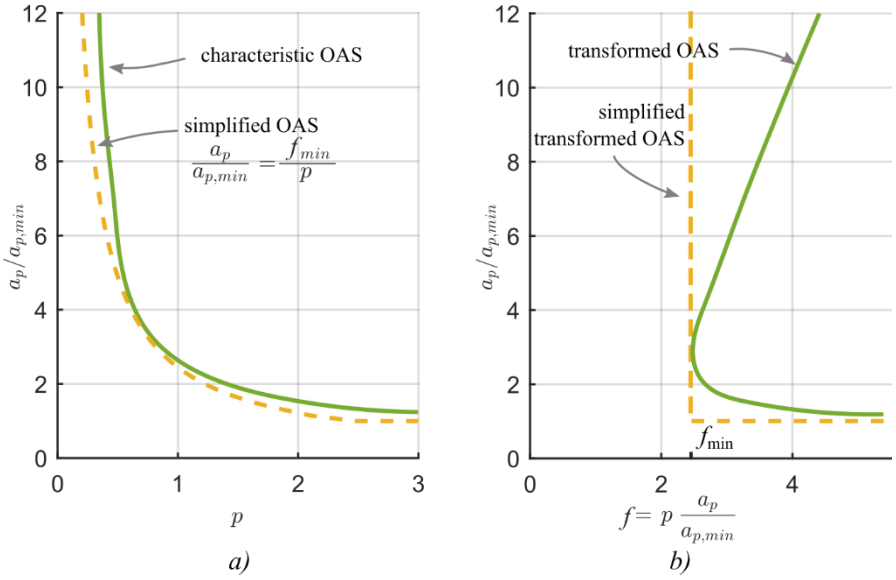

Fig. 47 An example of the characteristic OAS (a) and the transformed characteristic OAS (b). Simplified OAS are given with dashed line

To strengthen this statement the convex hulls of *OAS*-s of the individual earthquake records and their *transformed OAS* were determined (Fig. 48). These convex hulls are presented in Fig. 49a and b for FF and NF earthquakes. For the sake of comparison, each curve was normalized by its lowest horizontal value.

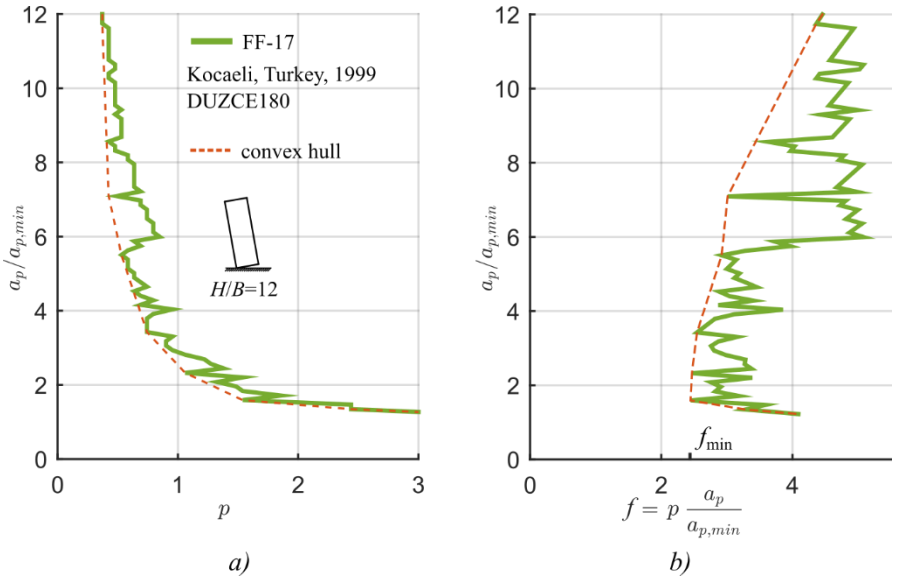

Fig. 48 An example OAS (a) and transformed OAS (b) with the corresponding convex hulls

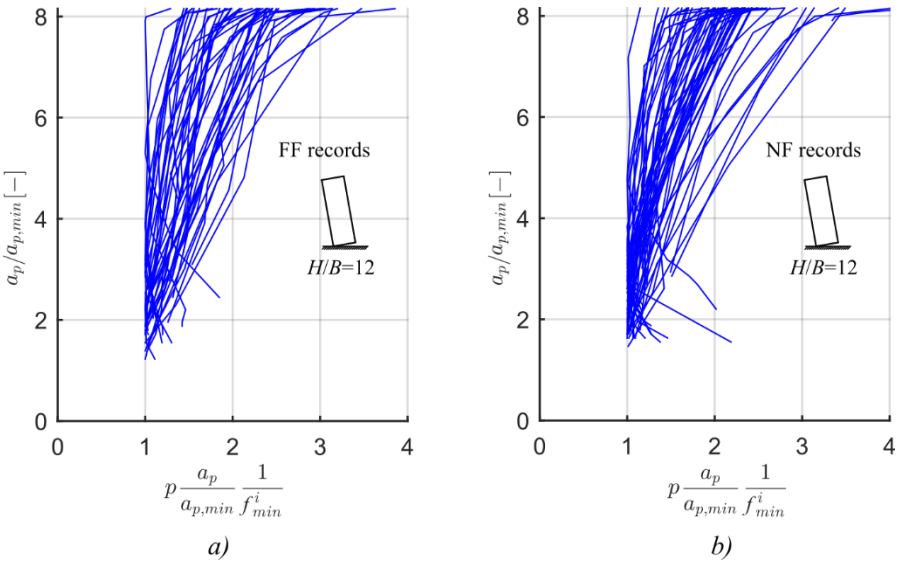

Fig. 49 Convex hulls of transformed OAS for far field (a) and near field (b) earthquakes normalized by their lowest horizontal coordinate

It is recommended that the transformed OAS is approximated by a horizontal and vertical line, by the *simplified transformed OAS*. The horizontal location of the vertical line (Fig. 47b) is given as a function of the normalized critical impulse Eq. (18)

$$f_{min} = \frac{i_{\mathrm{cr}}}{t_{\mathrm{I}}} = \frac{1}{t_{\mathrm{I}}}\sqrt{\frac{2}{1+\cos\delta}} \approx \frac{1}{t_{\mathrm{I}}}, \tag{20}$$

where t_{I} is the *'replacement impulse duration'*. Its value can be determined numerically, using the transformed OAS of real earthquake records.

It is recommended to represent earthquakes by two parameters: a_{p} and t_{I}.

On the basis of t_{I} the *simplified OAS* can be calculated as (Eq. (19)):

$$\frac{a_p}{a_{p,\min}} = \max\left\{\frac{i_{\mathrm{cr}}}{t_{\mathrm{I}}}\frac{1}{p}, 1\right\} \approx \max\left\{\frac{1}{t_{\mathrm{I}}}\frac{1}{p}, 1\right\}. \tag{21}$$

For the 100 investigated earthquakes we determined numerically the t_I values, their histograms are given in Fig. 50. The maximum values are t_I=0.686 and t_I=0.961 for far field and near field records, respectively. The corresponding records (FF-38 and NF-52) belong to the Chi-Chi earthquake (1999, Taiwan, CHICHI/CHY101-N and CHICHI/TCU102-N). The second biggest values are: t_I=0.540 for Landers (1992, LANDERS/YER360) and t_I=0.671 for Kocaeli, Turkey (1999, YARIMCA/60).

t_I values for all the investigated earthquakes are given in Table 4 and Table 5.

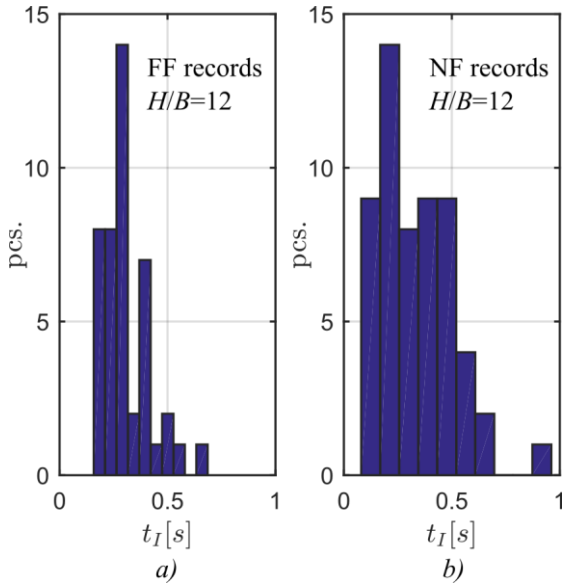

Fig. 50 Histograms of replacement impulse durations t_I for the FF (a) and the NF (b) records.

Table 4 The investigated FF earthquakes and the calculated pulse durations.

ID	Year	Event	Station	Direction	t_p [s]	t_I [s] H/B=12	t_I' H/B=12	β H/B=12
FF-1	1994	Northridge	Beverly Hills - Mulhol	009	0.405	0.266	0.387	1.744
FF-2	1994	Northridge	Beverly Hills - Mulhol	279	0.367	0.360	0.538	1.467
FF-3	1994	Northridge	Canyon Country - WLC	000	0.269	0.302	0.479	1.407
FF-4	1994	Northridge	Canyon Country - WLC	270	0.219	0.285	0.347	1.933
FF-5	1999	Duzce, Turkey	Bolu	000	0.134	0.194	0.207	7.814
FF-6	1999	Duzce, Turkey	Bolu	090	0.241	0.203	0.287	1.203
FF-7	1999	Hector Mine	Hector	000	0.251	0.304	0.352	3.495
FF-8	1999	Hector Mine	Hector	090	0.228	0.299	0.434	2.117
FF-9	1979	Imperial Valley	Delta	262	0.293	0.473	0.624	3.800
FF-10	1979	Imperial Valley	Delta	352	0.294	0.421	0.643	3.283
FF-11	1979	Imperial Valley	El Centro Array #11	140	0.145	0.289	0.661	1.694
FF-12	1979	Imperial Valley	El Centro Array #11	230	0.185	0.228	0.330	3.086
FF-13	1995	Kobe, Japan	Nishi-Akashi	000	0.215	0.226	0.350	1.583
FF-14	1995	Kobe, Japan	Nishi-Akashi	090	0.187	0.225	0.276	2.211
FF-15	1995	Kobe, Japan	Shin-Osaka	000	0.330	0.305	0.462	1.864
FF-16	1995	Kobe, Japan	Shin-Osaka	090	0.331	0.367	0.445	2.811
FF-17	1999	Kocaeli, Turkey	Duzce	180	0.408	0.409	0.435	14.138
FF-18	1999	Kocaeli, Turkey	Duzce	270	0.292	0.376	0.665	2.217
FF-19	1999	Kocaeli, Turkey	Arcelik	000	0.104	0.158	~∞	1.200

FF-20	1999	Kocaeli, Turkey	Arcelik	090	0.294	0.412	~∞	2.720
FF-21	1992	Landers	Yermo Fire Station	270	0.438	0.483	0.630	4.832
FF-22	1992	Landers	Yermo Fire Station	360	0.425	0.540	0.672	4.543
FF-23	1992	Landers	Coolwater	LN	0.172	0.315	0.381	1.991
FF-24	1992	Landers	Coolwater	TR	0.300	0.259	0.322	1.856
FF-25	1989	Loma Prieta	Capitola	000	0.189	0.274	0.345	1.458
FF-26	1989	Loma Prieta	Capitola	090	0.208	0.272	0.331	1.573
FF-27	1989	Loma Prieta	Gilroy Array #3	000	0.155	0.242	0.310	1.488
FF-28	1989	Loma Prieta	Gilroy Array #3	090	0.200	0.242	0.350	2.476
FF-29	1990	Manjil, Iran	Abbar	L	0.148	0.270	0.602	1.703
FF-30	1990	Manjil, Iran	Abbar	T	0.145	0.405	0.606	2.020
FF-31	1987	Superstition Hills	El Centro Imp. Co.	000	0.263	0.290	0.320	7.286
FF-32	1987	Superstition Hills	El Centro Imp. Co.	090	0.250	0.403	0.772	2.838
FF-33	1987	Superstition Hills	Poe Road (temp)	270	0.165	0.189	0.346	1.492
FF-34	1987	Superstition Hills	Poe Road (temp)	360	0.193	0.281	0.324	5.077
FF-35	1992	Cape Mendocino	Rio Dell Overpass	270	0.267	0.249	0.365	1.431
FF-36	1992	Cape Mendocino	Rio Dell Overpass	360	0.215	0.175	0.264	0.945
FF-37	1999	Chi-Chi, Taiwan	CHY101	E	0.520	0.413	0.561	4.733
FF-38	1999	Chi-Chi, Taiwan	CHY101	N	0.654	0.686	1.036	3.736
FF-39	1999	Chi-Chi, Taiwan	TCU045	E	0.198	0.185	0.211	2.690
FF-40	1999	Chi-Chi, Taiwan	TCU045	N	0.209	0.165	0.318	1.335
FF-41	1971	San Fernando	LA - Hollywood Stor	090	0.224	0.503	0.897	1.841
FF-42	1971	San Fernando	LA - Hollywood Stor	180	0.155	0.312	0.371	2.663
FF-43	1976	Friuli, Italy	Tolmezzo	000	0.131	0.165	0.204	1.371
FF-44	1976	Friuli, Italy	Tolmezzo	270	0.267	0.228	0.309	1.256

Table 5 The investigated NF earthquakes and the calculated pulse durations

ID	Year	Event	Station	Direction	t_p [s]	t_l [s] H/B=12	t_l' H/B=12	β H/B=12	$T_p/2$ (Baker 2007)	$T_p/2$ (Mimoglou et al. 2014)
NF-1	1976	Gazli, USSR	Karakyr	000	0.157	0.247	0.332	2.500	-	
NF-2	1976	Gazli, USSR	Karakyr	090	0.163	0.163	0.270	1.694	-	
NF-3	1979	Imperial Valley	Bonds Corner	140	0.206	0.223	0.290	1.978	-	
NF-4	1979	Imperial Valley	Bonds Corner	230	0.173	0.237	0.341	1.134	-	
NF-5	1979	Imperial Valley	Chihuahua	012	0.208	0.344	0.568	2.022	-	
NF-6	1979	Imperial Valley	Chihuahua	282	0.285	0.362	0.539	1.910	-	
NF-7	1979	Imperial Valley	Chihuahua	DWN	0.070	0.111	0.120	2.552	-	
NF-8	1979	Imperial Valley	El Centro Array #6	230	**0.483**	**0.392**	0.569	4.794	**1.90**	**1.97**
NF-9	1979	Imperial Valley	El Centro Array #7	140	0.317	0.461	0.608	3.032	-	
NF-10	1979	Imperial Valley	El Centro Array #7	230	**0.382**	0.414	0.429	17.625	**2.10**	**1.72**
NF-11	1980	Irpina, Italy	Sturno	000	0.411	0.443	0.632	2.539	-	
NF-12	1980	Irpina, Italy	Sturno	270	**0.332**	**0.462**	0.654	3.071	**1.55**	**1.32**
NF-13	1985	Nahanni, Canada	Site 1	010	0.085	0.088	0.095	1.976	-	
NF-14	1985	Nahanni, Canada	Site 1	280	0.081	0.089	0.098	2.676	-	
NF-15	1985	Nahanni, Canada	Site 2	240	0.082	0.100	0.130	1.752	-	
NF-16	1985	Nahanni, Canada	Site 2	330	0.188	0.152	0.266	1.224	-	
NF-17	1987	Superstition Hills-02	Parachute Test Site	225	**0.655**	**0.570**	1.168	2.033	**1.15**	
NF-18	1987	Superstition Hills-02	Parachute Test Site	315	0.283	0.323	0.594	1.909	-	
NF-19	1989	Loma Prieta	Bran	000	0.264	0.238	0.312	1.949	-	
NF-20	1989	Loma Prieta	Bran	090	0.227	0.196	0.321	1.168	-	
NF-21	1989	Loma Prieta	Corralitos	000	0.206	0.171	0.613	0.919	-	
NF-22	1989	Loma Prieta	Corralitos	090	0.279	0.225	0.264	2.259	-	
NF-23	1989	Loma Prieta	Saratoga - Aloha Ave	000	**0.184**	**0.199**	0.221	3.502	**2.25**	**3.24**
NF-24	1989	Loma Prieta	Saratoga - Aloha Ave	090	0.189	0.317	0.358	5.012	-	
NF-25	1992	Erzica, Turkey	Erzican	EW	0.285	0.345	0.415	3.027	-	

NF-26	1992	Erzica, Turkey	Erzican	NS	**0.617**	**0.423**	0.720	2.383	**1.35**	**1.21**
NF-27	1992	Cape Mendocino	Cape Mendocino	000	0.155	0.080	0.083	7.916	-	
NF-28	1992	Cape Mendocino	Cape Mendocino	090	0.099	0.081	0.081	77.630	-	
NF-29	1992	Cape Mendocino	Petrolia	000	0.228	0.221	0.264	2.496	-	
NF-30	1992	Cape Mendocino	Petrolia	090	**0.299**	**0.244**	0.298	2.331	**1.50**	**1.37**
NF-31	1992	Landers	Lucerne	260	**0.137**	**0.246**	0.251	56.932	**2.55**	**2.29**
NF-32	1992	Landers	Lucerne	345	0.064	0.110	0.122	1.772	-	
NF-33	1994	Northridge	Sepulveda VA Hospital	270	0.323	0.241	0.334	1.361	-	
NF-34	1994	Northridge	Sepulveda VA Hospital	360	0.169	0.196	0.223	2.549	-	
NF-35	1994	Northridge	17645 Saticoy St	090	0.250	0.403	0.513	2.067	-	
NF-36	1994	Northridge	17645 Saticoy St	180	0.416	0.447	0.707	1.633	-	
NF-37	1994	Northridge	Rinaldi Receiving Station	228	**0.450**	**0.270**	0.401	2.390	**0.60**	**0.55**
NF-38	1994	Northridge	Rinaldi Receiving Station	318	0.400	0.387	0.841	1.140	-	
NF-39	1994	Northridge	Sylmar - Olive View Med FF	090	0.285	0.289	0.425	1.897	-	
NF-40	1994	Northridge	Sylmar - Olive View Med FF	360	**0.282**	**0.257**	0.438	1.756	**1.55**	**1.28**
NF-41	1999	Kocaeli, Turkey	Izmit	090	0.254	0.252	0.454	3.085	-	
NF-42	1999	Kocaeli, Turkey	Izmit	180	0.288	0.376	0.786	1.795	-	
NF-43	1999	Kocaeli, Turkey	Yarimca	060	0.703	0.671	1.703	3.249	-	
NF-44	1999	Kocaeli, Turkey	Yarimca	150	0.478	0.443	0.554	6.490	-	
NF-45	1999	Chi-Chi, Taiwan	TCU065	E	0.344	0.381	0.553	4.656	-	
NF-46	1999	Chi-Chi, Taiwan	TCU065	N	**0.352**	**0.504**	0.840	3.697	**2.85**	**2.37**
NF-47	1999	Chi-Chi, Taiwan	TCU067	E	0.439	0.461	1.107	2.464	-	
NF-48	1999	Chi-Chi, Taiwan	TCU067	N	0.485	0.545	0.742	3.564	-	
NF-49	1999	Chi-Chi, Taiwan	TCU084	E	0.369	0.342	0.475	1.827	-	
NF-50	1999	Chi-Chi, Taiwan	TCU084	N	0.312	0.337	0.552	2.290	-	
NF-51	1999	Chi-Chi, Taiwan	TCU102	E	0.834	0.583	0.987	4.994	-	
NF-52	1999	Chi-Chi, Taiwan	TCU102	N	**1.176**	**0.961**	2.117	3.982	**4.85**	**4.65**
NF-53	1999	Duzce, Turkey	Duzce	180	0.298	0.500	0.671	3.600	-	
NF-54	1999	Duzce, Turkey	Duzce	270	0.335	0.466	0.585	4.733	-	
NF-55	2002	Denali, Alaska	TAPS Pump Station #10	047	0.849	0.649	0.829	4.744	-	
NF-56	2002	Denali, Alaska	TAPS Pump Station #10	317	0.565	0.547	~∞	1.740	-	

5.3.3 Generalization for arbitrary symmetrical mass distribution

In the previous sections it was assumed that the mass of the block is uniformly distributed over a rectangular area. Note, however, that the derived expressions can be applied for arbitrary, symmetrical mass distribution. We define a dimensionless α parameter in the following way (see Eq. (13)):

$$\Theta = \alpha m R^2 \tag{22}$$

where Θ is the mass moment of inertia about the corner point where the rotation occurs, m is the total mass and R is the distance between the center of mass and the corner point. In case of uniform mass distribution α=4/3 (see Eq. (13)). Three examples are shown in Fig. 51. Housner's approximate expression for the natural period of vibration Eq. (14), the expression of the critical impulse Eq. (17) are directly applicable to these cases if the proper value of α is introduced, while the expression of $a_{p,min}$ Eq. (3) does not change. We may also observe that all performed calculations for OAS and transformed OAS are also valid, if the proper value of α is used.

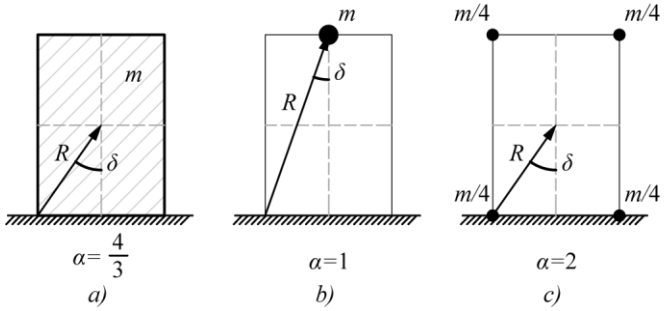

Fig. 51 Values of α for different mass distributions to calculate the mass moment of inertia in Eq. (22)

5.3.4 Numerical example

To demonstrate the simplicity of the recommended procedure we give an example in which we determine the required width of a pier at an undefined location.

The required safety against overturning is not the subject of this paper. Here we take a_g=0.14 g as the PGA, and t_I=0.7 s as the *design replacement impulse duration*. (The latter one is the highest value of the 44 investigated FF records.).

(a) Determine the necessary width (B_a) of an H=12 m solid pier!

(b) Determine the necessary width (B_b), if the mass is at the top of the pier and the weight of the pier is neglected!

Note that for B_a =1.68 m and B_b =3.36 m we have $a_p = a_{p,min}$, and the pier will not move.

The pier can be, however, narrower. Eq. (21) for the two cases are:

$$\frac{a_g}{\frac{gB_a}{H}} = \frac{1}{t_I}\sqrt{\frac{4}{3}\frac{\sqrt{\left(\frac{B_a}{2}\right)^2+\left(\frac{H}{2}\right)^2}}{g}}, \qquad \frac{a_g}{\frac{gB_b}{2H}} = \frac{1}{t_I}\sqrt{\frac{\sqrt{\left(\frac{B_b}{2}\right)^2+H^2}}{g}}. \tag{23}$$

Eqs (23) are nonlinear, which result in B_a =1.299 m and B_b =2.122 m.

If the blocks are slender ($\cos\delta \approx 1$), the above expressions simplify to

$$B_a \approx \sqrt{H}t_I\frac{a_g}{\sqrt{g}}\sqrt{\frac{3}{2}}, \quad B_b \approx \sqrt{H}t_I\frac{a_g}{\sqrt{g}}2, \tag{24}$$

which results in B_a =1.302 m and B_b =2.127 m.

5.3.5 Discussion

The replacement impulse duration

It is worthwhile to compare the calculated *replacement impulse durations* to the parameters of the main pulse lobes of real earthquake records. To reach this goal we made a very simple calculation shown below. Overturning may be caused by either a large acceleration (a_{max}) or by a large impulse (I_{max}), the corresponding pulses are shown by shaded areas in Fig. 52a. (They may coincide.) To capture both we defined a single pulse as a simple sine curve with a_{max} and I_{max} (Fig. 52b). The fullness of a sine curve is F=0.64, and its duration is:

$$t_p = \frac{I_{max}}{Fa_{max}}. \tag{25}$$

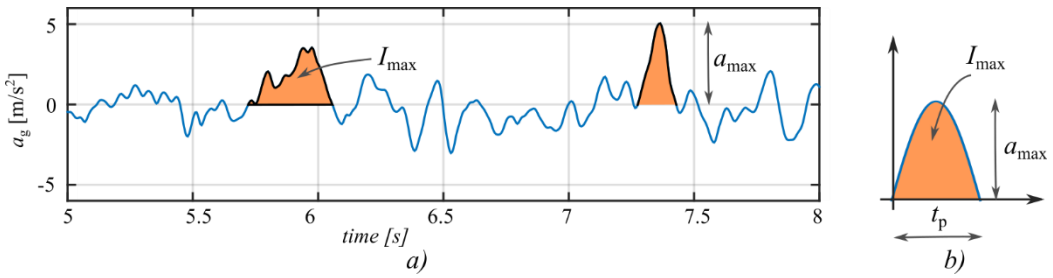

Fig. 52 An acceleration record and the definition of a_{max} and $I_{max,}$(a), and the replacement sine curve (b). The record is the 1979, Imperial Valley – Bonds Corner/140 (NF-3)

The t_p values corresponding to each earthquakes are given in Table 4 and Table 5. We investigated the correlation between t_I and $t_{p,}$ (Fig. 53), and found high correlation, higher for NF than for FF records. Interestingly, linear regression gives approximately $t_I \approx (0.8 \div 1)t_p$. Note that for simple signals (Fig. 46 b-d) we obtain $t_I \approx (0.75 \div 0.9)t_p$.

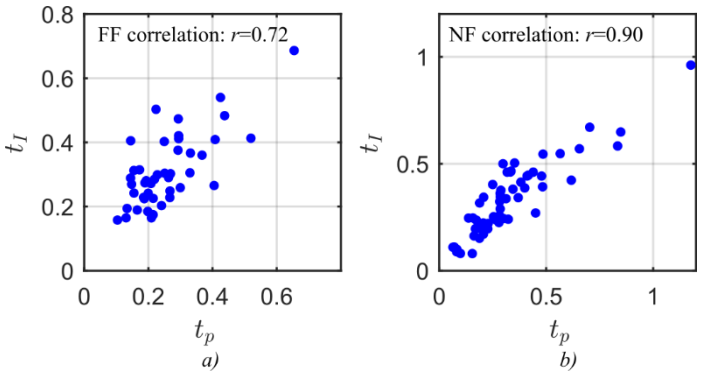

Fig. 53 The corresponding t_I and t_p values for the FF (a) and the NF (b) records. The correlation coefficients are 0.72 and 0.90 for FF and NF, respectively

We may observe that these 'replacement' durations are much shorter than those which were defined in a more sophisticated way by researchers (Mavroeidis and Papageorgiou 2003; Baker 2007; Vassiliou and Makris 2011; Mimoglou et al. 2014) for NF fault-parallel records, on the basis of the pulse durations in the velocity record (see in Table 5). We also compared those values with t_I, however, they seem to be uncorrelated.

Representation of the results

In Fig. 54 the results are presented in four different ways. The solid line represents the accurate solution, while the dashed line the simple approximation (Eq. (21)). (Note that $a_{p,min}$ is proportional to the inverse of the slenderness and p depends on the element size.) For $a_p > a_{p,min}$ the approximate relationship between $a_{p,min}$ and p is linear:

$$a_{p,min} = a_p t_I p. \tag{26}$$

Note that for an infinitely short impulse the accurate expression is also linear (Eq. (17)):

$$a_{p,min} = I_{cr} p. \tag{27}$$

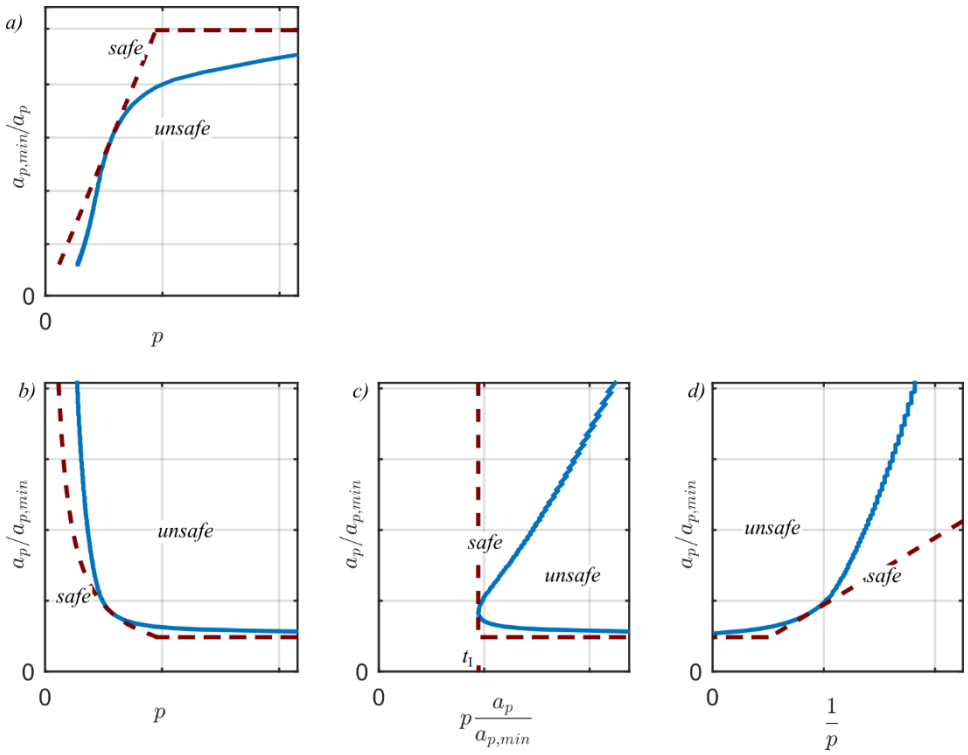

Fig. 54 Representation of the overturning acceleration spectra for an arbitrary pulse

Improved approximation

In Fig. 55 we present our proposed solution Eq. (21) for a real earthquake record. For the sake of comparison to curves presented by other researchers (Zhang and Makris 2001; Makris and Konstantinidis 2003; Makris and Vassiliou 2012; Dimitrakopoulos and DeJong 2012; Dimitrakopoulos and Fung 2016), we give the results also as a function of 1/*p* (Fig. 55c). Note that the contents of the three plots (a-c) are identical, the difference is only in the presentation.

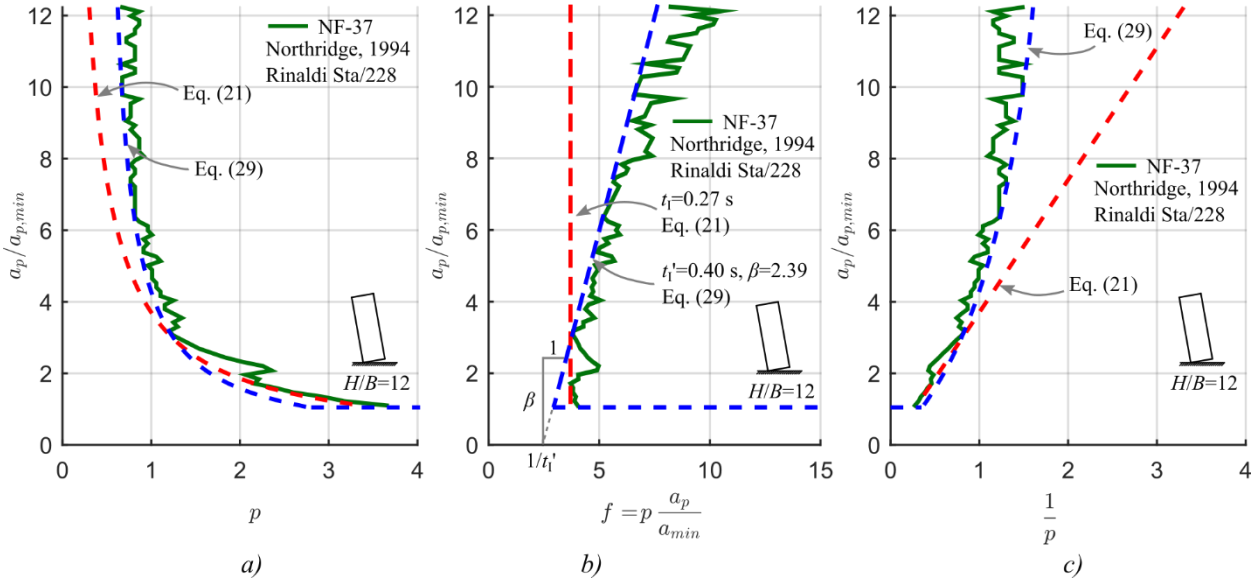

Fig. 55 OAS (a), transformed OAS (b) and OAS as a function of 1/p (c) for the Northridge earthquake compared to simplified curves (t_1=0.27, t_1' =0.40, β=2.39)

As we mentioned before, instead of the vertical line in Fig. 55b (Fig. 37b, Fig. 47b), we may approximate the *transformed OAS* by an inclined line, which can be defined by two parameters: t_I' and the slope of the inclined line, β. By so doing we arrive at the following expression:

$$p\frac{a_p}{a_{p,min}} = \frac{a_p}{a_{p,min}}\frac{1}{\beta} + \frac{1}{t'_I} \tag{28}$$

which results in

$$\frac{a_p}{a_{p,min}} = \max\left\{\frac{1}{t'_I}\frac{1}{p-1/\beta}; 1\right\} \tag{29}$$

For most cases this equation gives a rather good approximation (marked by blue dashed lines in Fig. 55), however, for the price of having two parameters instead of only one. Finally, to achieve a better fit, we may approximate the *transformed OAS* by a vertical and an inclined line, which results in

$$\frac{a_p}{a_{p,min}} = \max\left\{\frac{1}{t_I}\frac{1}{p}; \frac{1}{t'_I}\frac{1}{p-1/\beta}; 1\right\}. \tag{30}$$

Comparisons for all the 100 investigated earthquake records are presented on our webpage (*http://www.szt.bme.hu/files/TherT/public_Eq21Eq29_Ther_Thesis.zip*). Eq. (30) is always very accurate (if $a_p/a_{p,min}<12$), while Eq. (21) provides reasonable results, if $a_p<4\text{-}6a_{p,min}$. Both approximations are conservative in the whole parameter range.

Comparison with the results obtained from single pulses

We compared our results with those obtained from realistic, single pulses. In Fig. 56a-c OAS-s are presented for three earthquakes, together with OAS of pulses determined by Makris and Vasilliou (in Makris and Vassiliou (2012) see Fig. 4), and our simplified curves (Eqs. (21) and (29)). We may observe that in Fig. 56a the results obtained from the (orange) replacement signal are not conservative, while in Fig. 56b, c they are very conservative.

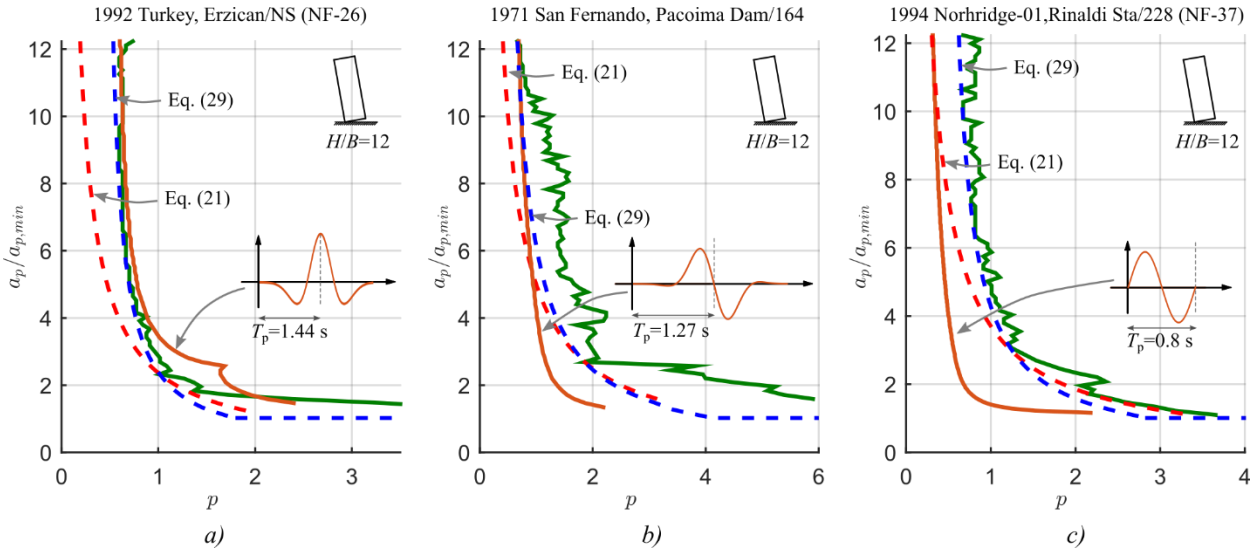

Fig. 56 The OAS of three different earthquakes compared to the results of single pulses (see Fig. 4 in (Makris and Vassiliou 2012)) and to our simplified equations (Eqs. (21) and (29))

Results for a given earthquake (see Fig. 56c) are also compared to the solution of Voyagaki et al. (2013a). In Fig. 57 the recommended solution of Voyagaki et al. (2013a) is presented, where the length of the

triangular signal was taken to be equal to $T_p/2=0.6$ s (Baker 2007). We may observe that Voyagaki's solution is unconservative.

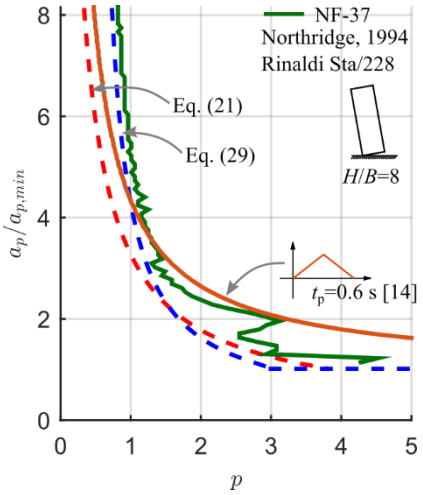

Fig. 57 OAS for the Northridge (NF-37) earthquake compared to the results of Voyagaki et al. (2013a)

The replacement signals were determined in the literature by analyzing the shape of earthquake records (Mavroeidis and Papageorgiou 2003; Baker 2007; Vassiliou and Makris 2011; Mimoglou et al. 2014). An alternative approach can be given considering the OAS instead of the earthquake record. Two examples are shown in Fig. 58. In both figures the envelope of the OAS of two signals are presented. The signals are given in Fig. 6d and g for Fig. 58a, and in Fig. 6e and f for Fig. 58b. Note that duration of the signals were determined not directly from the earthquake record, but on the basis of the OAS of the earthquake. We failed to find proper representations of earthquakes by using only one, simple signal; rather at least two signals had to be used.

One might argue that these shapes or durations have no physical justification, which might be true, however, their responses will be close to that of the earthquake, at least for overturning. Our aim was to demonstrate that with a few signals a reasonably good curve-fit can be achieved.

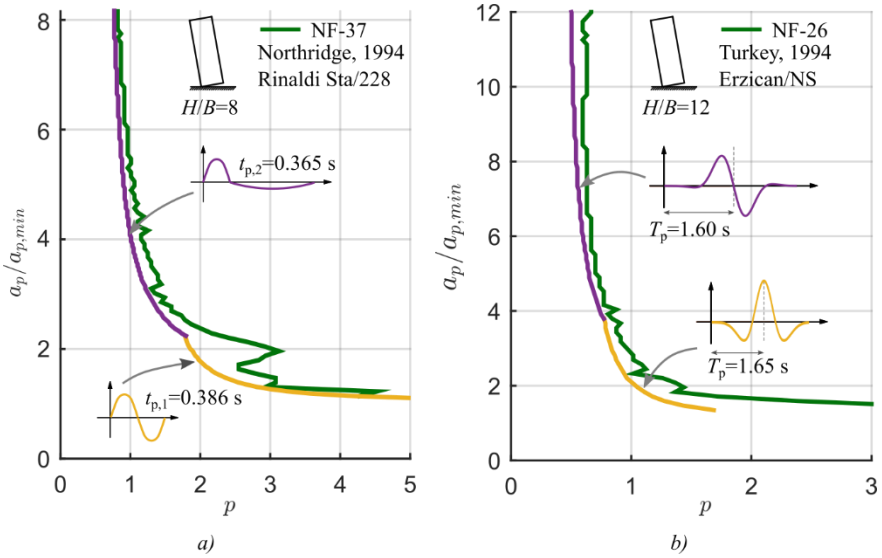

Fig. 58 The OAS for the Northridge (NF-37) earthquake compared to the results of two replacement signals (a). The envelope of the Erzican (NF-26) earthquake, using the replacement signals of Makris and Vassiliou (2012) (b)

5.4 Summary

The response spectrum analysis (RSA) cannot be used for the analysis and design of rigid blocks for overturning because the period of vibration of rocking mechanisms depends strongly on the amplitude of the rocking block.

The main finding is that the *overturning acceleration spectrum* (OAS) can be used to represent the effect of earthquakes for the analysis of overturning of rigid blocks. A *characteristic OAS* can be determined by the statistical evaluation of time history analyses of rocking mechanisms for earthquake records at a given location.

Our second important finding, based on the analyses of rigid blocks for 100 earthquake records, is that the OAS can be characterized reasonably well by one parameter: the *replacement impulse duration* t_I, which plays a similar role as the T_B, T_C, etc. points of the (pseudo) acceleration response spectrum of the RSA. If t_I and the maximum acceleration a_p are given for a location we can determine whether a column is safe against overturning simply by checking the following inequalities (Eq.(21)):

$$a_p \le a_{p,min} \frac{1}{t_I} \sqrt{\alpha \frac{R}{g}} \quad \text{or} \quad a_p \le a_{p,min} \tag{31}$$

(We may obtain a better approximation by using additional parameters t'_p and β (see Table 4, Table 5 and Eq. (29).)

It was also demonstrated that for the analysis of overturning of rigid blocks the effect of complex earthquakes can be reasonably well represented by the envelope of a few (in the examples two) simple signals (Fig. 58), where the durations of the signals are determined from the OAS (or from the simplified OAS). This procedure is analogous to the time history analysis of standards (e.g. EC8), where earthquake records are selected to match a target response spectrum curve.

The calculation of the *replacement impulse duration* t_I for a specific site is not the subject of our research. Nevertheless, results for 100 individual records are presented. We must emphasize that t_I may depend strongly on the soil parameters above the bedrock.

Chapter 6 Conclusion – New results

Housner derived a model for rocking mechanisms, which gives the change of angular velocities (and the energy loss) during impact (Housner 1963). This model is widely used (Augusti and Sinopoli 1992; Lipscombe and Pellegrino 1993; Makris and Konstantinidis 2003; Prieto et al. 2004; Makris and Vassiliou 2012; Dimitrakopoulos and DeJong 2012; Kounadis 2015) even though experiments show lower energy loss. Several researchers investigated this discrepancy in the last five decades (Aslam et al. 1980; Yim et al. 1980; Lipscombe and Pellegrino 1993; Anooshehpoor and Brune 2002; Ma 2010; Elgawady et al. 2011), however no reasonable physical explanations were given, and besides suggesting to use a fudge factor (Priestley et al. 1978; Aslam et al. 1980; Lipscombe and Pellegrino 1993; Anooshehpoor and Brune 2002; Elgawady et al. 2011) no numerical model was recommended.

Thesis 1. A new physical explanation was given for the difference between the results of Housner's model and the experiments: Impact does not occur at the edges of the block, rather, due to the unevenness of the surface, with consecutive impacts (Ther and Kollár 2017d).

1.1 The above hypothesis was verified by experiments on granite blocks. When two steel wires were glued to the edges the experiments agreed well with Housner's prediction, while gave lower energy loss for three wires, or when no wires were introduced.

1.2 For numerical calculations it was suggested that impact is modelled by assuming two consecutive impacts, the first at the middle, and the second at the edge. This model gives similar results as most of the experiments reported in the literature (Ogawa 1977; Aslam et al. 1980; Prieto-Castrillo 2007).

Impact models are available for single blocks (Housner 1963) and two-block columns (Psycharis 1990; Spanos et al. 2001), no model is available for multi-block columns with more than two blocks.

Thesis 2. A new impact model is developed for 2D multi-block columns, which enable us to calculate the change of velocities during impacts. The key of the model is that in formulating the problem at the closing interface both the clockwise and counter-clockwise rotations are taken into account, even though these motions exclude each other (Ther and Kollár 2017b). For one or two blocks this new model simplifies to those of (Housner 1963) and (Psycharis 1990).

After impact of multi-block columns several different opening configurations (crack-patterns) may occur. These were investigated only for two-block columns (Psycharis 1990; Spanos et al. 2001). More importantly, the possibility of different kinematically admissible opening configurations were not even mentioned.

Thesis 3. A model was developed to investigate the actual opening scheme of multi-block columns during impact (Ther and Kollár 2017b). The kinematically admissible opening configurations are chosen by investigating the signs of post-impact velocities, and then the one is considered, where the kinetic energy is the highest (the energy loss is the lowest). The model was validated by experiments.

When an interface of multi-block columns opens up several different opening configurations may occur. These were not investigated before.

Thesis 4. It was shown that simple opening of an interface where the thrust line is outside of the cross-section may be numerically unstable. A model was developed to investigate the actual opening configuration of multi-block columns (Ther and Kollár 2017b). The kinematically admissible configurations are chosen by investigating the signs of displacements. The model was validated by experiments.

Mechanical models to calculate the motion of multi-block columns are available only for given crack-patterns (Prieto-Castrillo 2007).

Thesis 5. A new model is developed (Ther and Kollár 2017b) for rocking of multi-block columns, which contains an opening and an impact model, together with the improved Housner's model presented in Thesis 1.2.

5.1 The model was verified by experiments.

5.2 Investigating columns for pulse-like signals and real earthquake records, it was found that monolithic blocks are more vulnerable for overturning than multi-block structures.

5.3 In contradiction to monolithic blocks, it was found that for multi-block columns the dissipation of energy during impact plays an important role.

For the design of blocks for single pulse-like signals the overturning curve (OC) was introduced (Housner 1963).

Thesis 6. The OC was generalized for earthquake records, and the *overturning acceleration spectrum* (OAS) was introduced (Ther and Kollár 2017c). In principle a *characteristic OAS* can be determined by the statistical evaluation of time history analyses of rocking mechanisms for earthquake records at a given location.

6.1 Based on the analyses of rigid blocks for 100 earthquake records, it was found that the OAS can be characterized well by one parameter: the "*replacement impulse duration*". It was also shown that the *replacement impulse durations* and the actual impulse durations of the main pulses of earthquake records are highly correlated.

6.2 A simple design equation was recommended to determine the safety of structures subjected to earthquakes for overturning.

Future works

As an extension of our column model, we are planning to develop a multi-block 2D arch model. In the literature, the masonry arch is investigated as a four-hinge mechanism for pulses and earthquake excitations (De Lorenzis 2007; DeJong et al. 2008; DeJong 2009). This system is a single degree of freedom structure.

Due to our preliminary calculations the locations and the number of open interfaces change during the motion of the structure which might influence the results. We plan to explore this question and to develop OAS-s for arches.

Appendices

Appendix A. Impact when the two axes of rotation are at arbitrary locations

Here, we give the simple extension of Housner's model, when the location of the axis of rotation before impact (P_1) and after the impact (P_2) are not at the edges of the block but at arbitrary positions (Fig. 59). Immediately before impact (rotation around axis P_1) the angular momentum about axis P_2 is

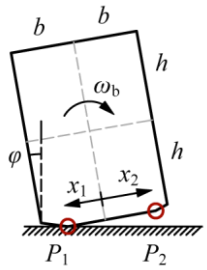

Fig. 59 Housner's model for a rocking block if rotation occurs around two axes of arbitrary position

$$L_{\mathrm{b}} = m\omega_b\left(\frac{(2b)^2}{12}+\frac{(2h)^2}{12}+h^2+x_1x_2\right) \tag{A1}$$

while after impact (rotation around axis P_2) the moment of momentum about axis P_2 is:

$$L_{\mathrm{a}} = m\omega_a\left(\frac{(2b)^2}{12}+\frac{(2h)^2}{12}+h^2+x_2^2\right) \tag{A2}$$

where m is the mass of the block, and x_1 and x_2 are the locations of the axes measured from the middle of the edge. From the condition that $L_a = L_b$, we obtain the following expression for the angular velocity:

$$\omega_{\mathrm{a}} = \mu\omega_{\mathrm{b}}, \qquad \mu = \frac{2h^2+0.5b^2+1.5x_1x_2}{2h^2+0.5b^2+1.5x_2^2} \tag{A3}$$

For $x_1 = -b$ and $x_2 = b$ Eqs.(1) and (A3) are identical.

If the corners are cut (Fig. 59), and we set $x_1 = -b_2$ and $x_2 = b_2$, Eq.(A3) results in

$$\omega_{\mathrm{a}} = \mu_{\mathrm{Hous}}\omega_{\mathrm{b}}, \qquad \mu_{\mathrm{HousC}} = \frac{2h^2+0.5b^2-1.5b_2^2}{2h^2+0.5b^2+1.5b_2^2} \tag{A4}$$

Now we apply Eq.(A3) in two steps. First, $x_1 = -b_2$ and $x_2 = 0$, i.e. the block rotates at the left corner and then impact occurs at the middle. This gives:

$$\omega_{\mathrm{a1}} = \omega_{\mathrm{b1}} \tag{A5}$$

and second: $x_1 = 0$ and $x_2 = b_2$, i.e. the block rotates at the middle and then impact occurs at the right corner:

$$\omega_{\mathrm{a2}} = \omega_{\mathrm{b2}}\frac{2h^2+0.5b^2}{2h^2+0.5b^2+1.5b_2^2} \tag{A6}$$

By setting $\omega_a = \omega_{a2}$, $\omega_b = \omega_{b1}$, $\omega_{a1} = \omega_{b2}$, from Eqs.(A5) and (A6) we obtain an expression for the change in the angular velocity, if rocking occurs in two steps, according to the geometry shown in Fig. 13b:

$$\omega_{\mathrm{a}} = \mu_{\mathrm{HousC}}^{\mathrm{2imp}}\omega_{\mathrm{b}}, \qquad \mu_{\mathrm{HousC}}^{\mathrm{2imp}} = \frac{2h^2+0.5b^2}{2h^2+0.5b^2+1.5b_2^2} \tag{A7}$$

If the width of the block is identical to the width of the base ($b = b_2$) Eq.(A7) simplifies to

$$\omega_{\mathrm{a}} = \mu_{\mathrm{HousC}}^{\mathrm{2imp}}\omega_{\mathrm{b}}, \qquad \mu_{\mathrm{HousC}}^{\mathrm{2imp}} = \frac{2h^2+0.5b^2}{2h^2+2b^2} \tag{A8}$$

Appendix B. Model of impact

Here the inelastic impact at a single point is discussed (Housner 1963), when the bumped elements may move together after impact. A structure has *m* degrees of freedom. The equation of motion is (Chopra 1995)

$$\mathbf{Ku} + \mathbf{C\dot{u}} + \mathbf{M\ddot{u}} = \mathbf{p}, \tag{B1}$$

where dot denotes derivation with respect to time, **K**, **M** and **C** are the $m \times m$ stiffness, mass and damping matrices, respectively. We assume that before impact the displacement vector is $\mathbf{u}^{\text{before}}$ while after impact it is denoted by $\mathbf{u}^{\text{after}}$. Impact occurs in a short time between t_0 and t_0+Δt. Eq.(B1) is integrated over this period

$$\mathbf{K}\int_{t_0}^{t_0+\Delta t}\mathbf{u}dt + \mathbf{C}\int_{t_0}^{t_0+\Delta t}\dot{\mathbf{u}}dt + \mathbf{M}\int_{t_0}^{t_0+\Delta t}\ddot{\mathbf{u}}dt = \int_{t_0}^{t_0+\Delta t}\mathbf{p}dt. \tag{B2}$$

During impact the change in velocity is $\Delta\mathbf{v} = \int_{t_0}^{t_0+\Delta t}\ddot{\mathbf{u}}dt$, the impulse is $\Delta\mathbf{I} = \int_{t_0}^{t_0+\Delta t}\mathbf{p}dt$, while the first two terms tend to zero with Δt. From Eq.(B2) when $\Delta t \to 0$ we obtain

$$\mathbf{M}\Delta\mathbf{v} = \Delta\mathbf{I}. \tag{B3}$$

It is assumed that impact occurs at the *i*th element of the displacement vector, i.e. $\dot{u}_i^{\text{after}} = 0$, and

$$\Delta v_i = -\dot{u}_i^{\text{before}}. \tag{B4}$$

The elements of $\Delta\mathbf{I}$ also tend to zero with Δt, except the *i*th one, since high contact forces arise during impact, and Eq.(B3) has the following form:

$$\begin{bmatrix} m_{1,1} & m_{1,2} & \dots & \dots & \dots & \dots & m_{1,\mathrm{m}} \\ m_{2,1} & m_{2,2} & & & & & \\ \vdots & & \ddots & & & & \\ \vdots & & & \ddots & & & \\ \vdots & & & & \ddots & & \\ \vdots & & & & & \ddots & \\ m_{\mathrm{m},1} & & & & & & m_{\mathrm{m,m}} \end{bmatrix} \begin{Bmatrix} \Delta v_1 \\ \Delta v_2 \\ \vdots \\ \Delta v_i \\ \vdots \\ \Delta v_m \end{Bmatrix} = \begin{Bmatrix} 0 \\ \vdots \\ 0 \\ \Delta I_i \\ 0 \\ \vdots \\ 0 \end{Bmatrix}. \tag{B5}$$

Disregarding the *i*th row of the above equation, and solving Eq.(B5) we obtain

$$\begin{Bmatrix} \Delta v_1 \\ \vdots \\ \Delta v_{i-1} \\ \Delta v_{i+1} \\ \vdots \\ \Delta v_m \end{Bmatrix} = \begin{bmatrix} m_{1,1} & \dots & m_{1,\mathrm{i-1}} & m_{1,\mathrm{i+1}} & \dots & m_{1,\mathrm{m}} \\ \vdots & \ddots & \vdots & \vdots & \ddots & \vdots \\ m_{\mathrm{i-1},1} & \dots & m_{\mathrm{i-1,i-1}} & m_{\mathrm{i-1,i+1}} & \dots & m_{\mathrm{i-1,m}} \\ m_{\mathrm{i+1},1} & \dots & m_{\mathrm{i+1,i-1}} & m_{\mathrm{i+1,i+1}} & \dots & m_{\mathrm{i+1,m}} \\ \vdots & \ddots & \vdots & \vdots & \ddots & \vdots \\ m_{\mathrm{m},1} & \dots & m_{\mathrm{m,i-1}} & m_{\mathrm{m,i+1}} & \dots & m_{\mathrm{m,m}} \end{bmatrix}^{-1} \begin{Bmatrix} m_{1,i} \\ \vdots \\ m_{i-1,i} \\ m_{i+1,i} \\ \vdots \\ m_{m,i} \end{Bmatrix} \Delta v_i, \tag{B6}$$

while Δv_i is given by Eq.(B4).

It may be observed that applying Eq.(B6) for one rectangular block the result is identical to that of Housner (Housner 1963). When the size of the block is 2*h* and 2*b*, the mass matrix is

$$\mathbf{M} = \begin{bmatrix} \Theta_0 & \Theta_1 \\ \Theta_1 & \Theta_0 \end{bmatrix}, \quad \Theta_0 = \frac{4}{3}m(h^2 + b^2), \quad \Theta_1 = \frac{4}{3}m\left(h^2 - \frac{1}{2}b^2\right). \tag{B7}$$

When $\breve{\varphi}_1$ is closing and $\hat{\varphi}_1$is opening, the change in velocity (Eq.(B6)):

$$\dot{\hat{\varphi}}_1 = {\Theta_0}^{-1}\Theta_1\dot{\breve{\varphi}}_1 = \frac{\Theta_1}{\Theta_0}\dot{\breve{\varphi}}_1 = \frac{1 - 0.5(b/h)^2}{1 + (b/h)^2}\dot{\breve{\varphi}}_1 \tag{B8}$$

which agrees with Housner's results.

Appendix C. Transformation of the equation of motion

The equation of motion of an elastic system with *n* degrees of freedom assuming small displacements is

$$\mathbf{K}\mathbf{u} + \mathbf{C}\dot{\mathbf{u}} + \mathbf{M}\ddot{\mathbf{u}} = \mathbf{p} \tag{C1}$$

where **u** and **p** are the vector of displacements and loads with *n* elements, **K**, **C** and **M** are the $n \times n$ stiffness, damping and mass matrices, respectively.

It is assumed that some of the displacements are not independent (e.g. parts of the structures – as rigid bodies – move together) and hence the actual degrees of freedom, denoted by *m* is smaller than *n*. The vector of the independent displacements is denoted by $\tilde{\mathbf{u}}$, and (for small displacements) the transformation between **u** and $\tilde{\mathbf{u}}$ is given by matrix **B**:

$$\underbrace{\mathbf{u}}_{(n\times 1)} = \underbrace{\mathbf{B}}_{(n\times m)}\ \underbrace{\tilde{\mathbf{u}}}_{(m\times 1)}. \tag{C2}$$

The strain energy and the kinetic energy of the system can be written as

$$U = \frac{1}{2}\mathbf{u}^{\mathrm{T}}\mathbf{K}\mathbf{u} = \frac{1}{2}\tilde{\mathbf{u}}^{\mathrm{T}}\underbrace{\mathbf{B}^{\mathrm{T}}\mathbf{K}\mathbf{B}}_{\tilde{\mathbf{K}}}\tilde{\mathbf{u}}, \tag{C3}$$

$$E_{\mathrm{kin}} = \frac{1}{2}\dot{\mathbf{u}}^{\mathrm{T}}\mathbf{M}\dot{\mathbf{u}} = \frac{1}{2}\dot{\tilde{\mathbf{u}}}^{\mathrm{T}}\underbrace{\mathbf{B}^{\mathrm{T}}\mathbf{M}\mathbf{B}}_{\tilde{\mathbf{M}}}\dot{\tilde{\mathbf{u}}}, \tag{C4}$$

where $\tilde{\mathbf{K}}$ and $\tilde{\mathbf{M}}$ are the reduced stiffness and mass matrices. The load vector of the motion must have the same length as $\tilde{\mathbf{u}}$, let us denote it by $\tilde{\mathbf{p}}$.

The work of external loads on the corresponding displacements must be identical for the original and for the reduced system:

$$W = \widetilde{W},\quad W = \mathbf{u}^{\mathrm{T}}\mathbf{p} = \tilde{\mathbf{u}}^{\mathrm{T}}\mathbf{B}^{\mathrm{T}}\mathbf{p},\quad \widetilde{W} = \tilde{\mathbf{u}}^{\mathrm{T}}\tilde{\mathbf{p}}, \tag{C5}$$

hence

$$\tilde{\mathbf{p}} = \mathbf{B}^{\mathrm{T}}\mathbf{p}. \tag{C6}$$

We substitute Eq.(C2) into Eq.(C1) and multiply it (from the left) by $\mathbf{B}^{\mathrm{T}}$. We obtain

$$\tilde{\mathbf{K}}\tilde{\mathbf{u}} + \tilde{\mathbf{C}}\dot{\tilde{\mathbf{u}}} + \tilde{\mathbf{M}}\ddot{\tilde{\mathbf{u}}} = \tilde{\mathbf{p}}, \tag{C7}$$

$$\tilde{\mathbf{K}} = \mathbf{B}^{\mathrm{T}}\mathbf{K}\mathbf{B},\qquad \tilde{\mathbf{M}} = \mathbf{B}^{\mathrm{T}}\mathbf{M}\mathbf{B},\qquad \tilde{\mathbf{C}} = \mathbf{B}^{\mathrm{T}}\mathbf{C}\mathbf{B} \tag{C8}$$

are the reduced stiffness, mass and damping matrices, respectively.

We may observe that for certain **p** loads $\mathbf{B}^{\mathrm{T}}\mathbf{p} = \mathbf{0}$, which means that this load does not affect the motion of the structure.

For the calculation of the multi-block cantilever each rigid block was represented by three mass points, which can accurately replace the mass, center of gravity and moment of inertia of a rigid body. Hence the original (Eq.(C1)) system has $n = 2 \times 3 \times n_{\mathrm{b}}$ equations, while the reduced one only $m = n_{\mathrm{b}}$. The **B** matrix was determined from geometrical considerations for arbitrary positions (Fig. C1) not only for the initial (straight) configuration.

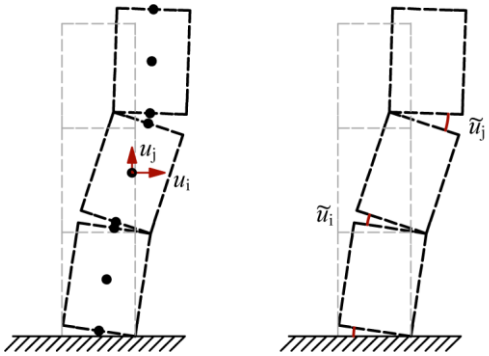

Fig. C1 The reduction of the degrees of freedom of the structure

The above procedure is illustrated below. Two blocks are placed on the top of each other in the initial (vertical) position (Fig. C2a). The sizes of each block are 1 by 4 meters and their mass is 1 kg. The mass of a block is concentrated at three nodal points, for this specific case their values are 0.177, 0.646 and 0.177 kg. Due to the 6 nodal points there are 12 degrees of freedom, the first six are the horizontal (x) displacement relative to the ground, and the last six are the vertical (y) displacements. The mass matrix is diagonal:

$$\mathbf{M} = \langle 0.177\ 0.646\ 0.177\ 0.177\ 0.646\ 0.177\ 0.177\ 0.646\ 0.177\ 0.177\ 0.646\ 0.177 \rangle. \tag{C9}$$

When the horizontal ground acceleration is -1 m/s^2 and the acceleration of gravity is 9.81 m/s^2, the load vector is:

$$\mathbf{p} = \begin{Bmatrix} 0.177 \\ 0.646 \\ 0.177 \\ 0.177 \\ 0.646 \\ 0.177 \\ -1.74 \\ -6.34 \\ -1.74 \\ -1.74 \\ -6.34 \\ -1.74 \end{Bmatrix} \text{[N]}. \tag{C10}$$

The first six elements are the horizontal, and the last six are the vertical components. The relationship between the nodal displacements and the rotations at the two interfaces (assuming small displacements) are (Eq.C2):

$$\mathbf{u} = \begin{Bmatrix} u_{x1} \\ u_{x2} \\ u_{x3} \\ u_{x4} \\ u_{x5} \\ u_{x6} \\ u_{y1} \\ u_{y2} \\ u_{y3} \\ u_{y4} \\ u_{y5} \\ u_{y6} \end{Bmatrix} = \mathbf{B}\tilde{\mathbf{u}} = \underbrace{\begin{bmatrix} 0 & 0 \\ -2.0 & 0 \\ -4.0 & 0 \\ -4.0 & 0 \\ -6.0 & -2.0 \\ -8.0 & -4.0 \\ -0.5 & 0 \\ -0.5 & 0 \\ -0.5 & 0 \\ -0.5 & -0.5 \\ -0.5 & -0.5 \\ -0.5 & -0.5 \end{bmatrix}}_{\mathbf{B}} \begin{Bmatrix} \tilde{u}_1 \\ \tilde{u}_2 \end{Bmatrix}, \tag{C11}$$

where the 12x2 matrix is identical to B. Its transpose, $\mathbf{B}^T$ is used to determine the new load vector (Eq.C6):

$$\tilde{\mathbf{p}} = \mathbf{B}^T\mathbf{p} = \begin{Bmatrix} 1.810 \\ 2.905 \end{Bmatrix} \text{ [Nm].} \tag{C12}$$

These are the moment couples at the axes of rotations (see Fig. C2a). (For the upper axis - 1×2+9.81×0.5=2.905 Nm.) The mass matrix of the reduced system is (Eq.C8):

$$\tilde{\mathbf{M}} = \mathbf{B}^T\tilde{\mathbf{M}}\mathbf{B} = \begin{bmatrix} 43.333 & 13.667 \\ 13.667 & 5.667 \end{bmatrix}. \tag{C13}$$

Now we investigate the case, when the upper block has an inclination of 10 degrees (Fig. C2b). The mass matrix and the load vector for the nodal points are identical to Eq.(C9) and (C10). The elements of the **B** matrix must be changed due to the new geometry:

$$\mathbf{u} = \begin{Bmatrix} u_{1x} \\ u_{2x} \\ u_{3x} \\ u_{4x} \\ u_{5x} \\ u_{6x} \\ u_{1y} \\ u_{2y} \\ u_{3y} \\ u_{4y} \\ u_{5y} \\ u_{6y} \end{Bmatrix} = \mathbf{B}\tilde{\mathbf{u}} = \begin{bmatrix} 0 & 0 \\ -2.0 & 0 \\ -4.0 & 0 \\ -4.087 & -0.087 \\ -6.056 & -2.056 \\ -8.026 & -4.026 \\ -0.5 & 0 \\ -0.5 & 0 \\ -0.5 & 0 \\ -0.492 & -0.492 \\ -0.145 & -0.145 \\ 0.202 & 0.202 \end{bmatrix} \begin{Bmatrix} \tilde{u}_1 \\ \tilde{u}_2 \end{Bmatrix}, \tag{C14}$$

and hence, the load vector and the mass matrix of the reduced system are also changed:

$$\tilde{\mathbf{p}} = \begin{Bmatrix} -1.728 \\ -0.633 \end{Bmatrix} \text{ [Nm],} \tag{C15}$$

$$\tilde{\mathbf{M}} = \begin{bmatrix} 43.785 & 13.892 \\ 13.892 & 5.667 \end{bmatrix}. \tag{C16}$$

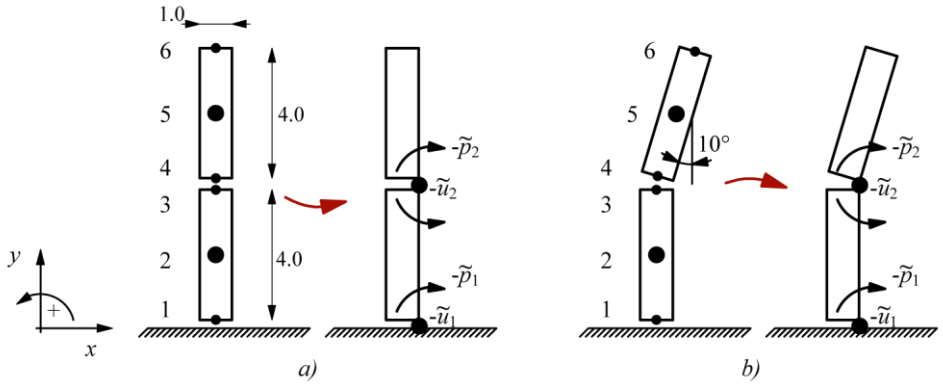

Fig. C2 Nodal points of a two block structure and the corresponding angular rotations and moment couples (positive if counterclockwise)

Acknowledgement

The authors gratefully thank the support of the OTKA 115673 project of the Hungarian National Research, Development and Innovation Office and the support of the TÁMOP - 4.2.2.B-10/1- 2010-0009 project for the usage of Superman, the supercomputer at the Budapest University of Technology and Economics.

References

Anooshehpoor A, Brune JN (2002) Verification of precarious rock methodology using shake table tests of rock models. Soil Dyn Earthq Eng 22:917–922. doi: 10.1016/S0267-7261(02)00115-X

Anooshehpoor A, Heaton TH, Shi B, Brune JN (1999) Estimates of the ground accelerations at Point Reyes Station during the 1906 San Francisco earthquake. Bull Seismol Soc Am 89:845–853.

Aslam M, Godden WG, Scalise DT (1980) Earthquake Rocking Response of Rigid Bodies. J Struct Div 106:377–392.

Augusti G, Sinopoli A (1992) Modelling the dynamics of large block structures. Meccanica 27:195–211. doi: 10.1007/BF00430045

Baker JW (2007) Quantitative classification of near-fault ground motions using wavelet analysis. Bull Seismol Soc Am 97:1486–1501. doi: 10.1785/0120060255

Chopra AK (1995) Dynamics of Structures. „Theory and applications to earthquake engeneering". Prentice Hall, Upper Saddle River, New Jersey

De Lorenzis L (2007) Failure of masonry arches under impulse base motion. Earthq Eng Struct Dyn 36:2119–2136. doi: 10.1002/eqe

DeJong M (2009) Seismic assessment strategies for masonry structures. MASSACHUSETTS INSTITUTE OF TECHNOLOGY

DeJong MJ (2012) Amplification of Rocking Due to Horizontal Ground Motion. Earthq Spectra 28:1405–1421. doi: 10.1193/1.4000085

DeJong MJ, De Lorenzis L, Adams S, Ochsendorf JA (2008) Rocking stability of masonry arches in seismic regions. Earthq Spectra 24:847–865. doi: 10.1193/1.2985763

Di Egidio a., Contento a. (2009) Base isolation of slide-rocking non-symmetric rigid blocks under impulsive and seismic excitations. Eng Struct 31:2723–2734. doi: 10.1016/j.engstruct.2009.06.021

Dimitrakopoulos EG, DeJong MJ (2012) Revisiting the rocking block: closed-form solutions and similarity laws. Proc R Soc A Math Phys Eng Sci 468:2294–2318. doi: 10.1098/rspa.2012.0026

Dimitrakopoulos EG, Fung EDW (2016) Closed-form Rocking Overturning Conditions for a Family of Pulse Ground Motions. Proc R Soc A. doi: 10.1098/rspa.2016.0662

Dimitri R, Lorenzis L De, Zavarise G (2011) Numerical study on the dynamic behavior of masonry columns and arches on buttresses with the discrete element method. Eng Struct 33:3172–3188. doi: 10.1016/j.engstruct.2011.08.018

Elgawady M, Ma Q, Butterworth JW, Ingham J (2011) Effects of interface material on the performance of free rocking blocks. Earthq Eng Struct Dyn 40:375–392. doi: 10.1002/eqe.1025

FEMA (2009) Quantification of building seismic performance factors. Federal Emergency Management Agency

Giouvanidis AI, Dimitrakopoulos EG (2017) Nonsmooth dynamic analysis of sticking impacts in rocking structures. Bull Earthq Eng 15:2273–2304. doi: 10.1007/s10518-016-0068-4

Heyman J (1966) The stone skeleton. Int J Solids Struct 2:249–279. doi: 10.1016/0020-7683(66)90018-7

Hogan SJ (1989) On the dynamics of rigid block motion under harmonic forcing. Proc R Soc London 425:441–476. doi: 10.1098/rspa.1989.0114

Hogan SJ (1992) On the Motion of a Rigid Block, Tethered at One Corner, under Harmonic Forcing. Proc R Soc A Math Phys Eng Sci 439:35–45. doi: 10.1098/rspa.1992.0132

Housner G (1963) The behavior of inverted pendulum structures during earthquakes. Bull Seismol Soc

Am 53:403–417.

Ishiyama Y (1982) Motions of Rigid Bodies and Criteria for Overturning By Earthquake Excitations. Earthq Eng Struct Dyn 10:635–650. doi: 10.1002/eqe.4290100502

Komodromos P, Papaloizou L, Polycarpou P (2008) Simulation of the response of ancient columns under harmonic and earthquake excitations. Eng Struct 30:2154–2164. doi: 10.1016/j.engstruct.2007.11.004

Konstantinidis D, Makris N (2005) Seismic response analysis of multidrum classical columns. Earthq Eng Struct Dyn 34:1243–1270. doi: 10.1002/eqe.478

Kounadis AN (2015) On the rocking-sliding instability of rigid blocks under ground excitation: some new findings. Soil Dyn Earthq Eng 75:246–258. doi: 10.1016/j.soildyn.2015.03.026

Lagomarsino S (2015) Seismic assessment of rocking masonry structures. Bull Earthq Eng 13:97–128. doi: 10.1007/s10518-014-9609-x

Lengyel G, Bagi K (2015) Numerical analysis of the mechanical role of the ribs in groin vaults. Comput Struct 158:42–60. doi: 10.1016/j.compstruc.2015.05.032

Lipscombe PR, Pellegrino S (1993) Free Rocking of Prismatic Blocks. J Eng Mech 119:1387–1410. doi: 10.1061/(ASCE)0733-9399(1993)119:7(1387)

Livesley RK (1978) Limit analysis of structures formed from rigid blocks. Int J Numer Methods … 12:1853–1871.

Ma QTM (2010) The mechanics of rocking structures subjected to ground motion. The University of Auckland, New Zealand

Makris N, Konstantinidis D (2003) The rocking spectrum and the limitations of practical design methodologies. Earthq Eng Struct Dyn 32:265–289. doi: 10.1002/eqe.223

Makris N, Vassiliou MF (2012) Sizing the slenderness of free-standing rocking columns to withstand earthquake shaking. Arch Appl Mech 82:1497–1511. doi: 10.1007/s00419-012-0681-x

Mavroeidis GP, Papageorgiou AS (2003) A mathematical representation of near-fault ground motions. Bull Seismol Soc Am 93:1099–1131. doi: 10.1785/0120020100

Mimoglou P, Psycharis IN, Taflampas IM (2014) Explicit determination of the pulse inherent in pulse-like ground motions. Earthq Eng Struct Dyn 43:2261–2281. doi: 10.1002/eqe.2446

Ogawa N (1977) A study on Rocking and Overturning of Rectangular Column." Report of the National Research Center for disaster Prevention(18), 14.

Oppenheim I (1992) The masonry arch as a four- link mechanism under base motion. Earthq Eng Struct Dyn 21:1005–1017.

Peña F, Prieto F, Lourenço PB, et al (2007) On the dynamics of rocking motion of single rigid-block structures. Earthq Eng Struct Dyn 36:2383–2399. doi: 10.1002/eqe.739

Peña F, Prieto F, Lourenço PB, Campos-Costa A (2006) Dynamical Behaviour of Rigid Block Structures Subjected to Earthquake Motion. Struct Anal Hist Constr 707–714. doi: 10.13140/2.1.2648.4166

Priestley MJN, Evision RJ, Carr a. J (1978) Seismic response of structures free to rock on their foundations. Bull New Zeal Soc Earthq Eng 11:141–150.

Prieto-Castrillo F (2007) On the dynamics of rigid-block structures applications to SDOF masonry collapse mechanisms. GUIMARÃES. Portugal: University of Minho

Prieto F, Lourenço PB, Oliveira CS (2004) Impulsive Dirac-delta forces in the rocking motion. Earthq Eng Struct Dyn 33:839–857. doi: 10.1002/eqe.381

Psycharis IN (1990) Dynamic behaviour of rocking two-block assemblies. Earthq Eng Struct Dyn

19:555–575. doi: 10.1002/eqe.4290190407

Psycharis IN, Papastamatiou DY, Alexandris AP (2000) Parametric investigation of the stability of classic al columns under harmonic and earthquake excitations. Earthq Eng Struct Dyn 29:1093–1109. doi: 10.1002/1096-9845(200008)29:8<1093::AID-EQE953>3.0.CO;2-S

Shi B, Anooshehpoor A (1996) Rocking and overturning of precariously balanced rocks by earthquakes. Bull Seismol Soc Am 86:1364–1371.

Sinopoli A (1991) Dynamic Analysis of a Stone Column Excited by a Sine Wave Ground Motion. Appl Mech Rev 44:S246. doi: 10.1115/1.3121361

Spanos PD, Koh A-S (1985) Rocking of Rigid Blocks Due to Harmonic Shaking. J Eng Mech 110:1627–1642. doi: 10.1061/(ASCE)0733-9399(1984)110:11(1627)

Spanos PD, Roussis PC, Politis NP a. (2001) Dynamic analysis of stacked rigid blocks. Soil Dyn Earthq Eng 21:559–578. doi: 10.1016/S0267-7261(01)00038-0

Szeidovitz G (1984) The Dunaharaszti Earthquake January 12, 1956. Acta Geod Geophys Mont Hung 21:109–125.

Ther T, Kollár LP (2017a) Refinement of Housner's model and its application for the overturning acceleration spectra. In: 16th World Conference on Earthquake Engineering,. Santiago, Chile,

Ther T, Kollár LP (2014) Response of Masonry Columns and Arches Subjected To Base Excitation. In: Ansal A (ed) Second European Conference on Earthquake Engineering and Seismology. Istanbul,

Ther T, Kollár LP (2017b) Model for Multi-Block Columns Subjected to Base Excitation. Earthq Eng Struct Dyn 1–19 accepted for publication.

Ther T, Kollár LP (2017c) Overturning of rigid blocks for earthquake excitation. Bull Earthq Eng 1–19 under review.

Ther T, Kollár LP (2017d) Refinement of Housner's model on rocking blocks. Bull Earthq Eng 15:2305–2319. doi: 10.1007/s10518-016-0048-8

Tóth A, Orbán Z, Bagi K (2009) Discrete element analysis of a stone masonry arch. Mech Res Commun 36:469–480. doi: 10.1016/j.mechrescom.2009.01.001

Vassiliou MF, Mackie KR, Stojadinović B (2016) A finite element model for seismic response analysis of deformable rocking frames. Earthq Eng Struct Dyn 1–6. doi: 10.1002/eqe.2799

Vassiliou MF, Makris N (2011) Estimating time scales and length scales in pulselike earthquake acceleration records with wavelet analysis. Bull Seismol Soc Am 101:596–618. doi: 10.1785/0120090387

Vassiliou MF, Truniger R, Stojadinović B (2015) An analytical model of a deformable cantilever structure rocking on a rigid surface: development and verificatio. Earthq Eng Struct Dyn. doi: 10.1002/eqe.2608

Voyagaki E, Psycharis IN, Mylonakis G (2013a) Complex Response of a Rocking Block to a Full-Cycle Pulse. J Eng Mech 4014024. doi: 10.1061/(ASCE)EM.1943-7889.0000712

Voyagaki E, Psycharis IN, Mylonakis G (2013b) Rocking response and overturning criteria for free standing rigid blocks to single—lobe pulses. Soil Dyn Earthq Eng 46:85–95. doi: 10.1016/j.soildyn.2012.11.010

Winkler T, Meguro K, Yamazaki F (1995) RESPONSE OF RIGID-BODY ASSEMBLIES TO DYNAMIC EXCITATION. Earthq Eng Struct Dyn 24:1389–1408. doi: 10.1002/eqe.4290241008

Yim C-S, Chopra AK, Penzien J (1980) Rocking Response of Rigid Blocks to Earthquakes. Earthq. Eng. Struct. Dyn. 8:565–587.

Zhang J, Makris N (2001) Rocking Response of Free-Standing Blocks under Cycloidal Pulses. J Eng Mech 127:473–483. doi: 10.1061/(ASCE)0733-9399(2001)127:5(473)

Zulli D, Contento A, Di Egidio A (2012) 3D model of rigid block with a rectangular base subject to pulse-type excitation. Int J Non Linear Mech 47:679–687. doi: 10.1016/j.ijnonlinmec.2011.11.004

(1956) Historia Domus, Taksony.